



ENHANCED INTERFACES AND TRAIN CATEGORIES FOR DYNAMIC COMPATIBILITY ASSESSMENT OF EUROPEAN RAILWAY BRIDGES

D5.1 – Revised acceleration criteria for railway bridges with ballastless tracks

DELIVERABLE INFORMATION				
Work package number:	WP5			
Work package title:	Revision of bridge deck acceleration limit			
Deliverable number:	D5.1			
Deliverable title:	Revised acceleration criteria for railway bridges with ballastless tracks			
Due date of deliverable:	28-02-2025			
Actual submission date of 1st version:	28-02-2025			
Current version submission date:	15-10-2025			
Responsible partner	UPORTO			
Version:	V2			
Dissemination level:	PU			



PUBLICATION HISTORY

Version	Date	Description	Responsible
V1	28-02-2025	Initial submission	P. Montenegro / UPORTO
V2	15-10-2025	Revised version after comments from the Reviewers sent on 24-09-2025. While no modifications were requested, some notes have been added based on the reviewers' comments.	P. Montenegro / UPORTO

CONTRIBUTORS TO THE DELIVERABLE

Name	Institution	Role
P. Montenegro	UPORTO	Deliverable co-responsible
G. Ferreira	UPORTO	Deliverable co-responsible
A. Henriques	UPORTO	Contributor
R. Calçada	UPORTO	Contributor
A. Andersson	KTH	Contributor
R. Karoumi	KTH	Contributor



PROJECT CONSORTIUM

Coordinator	Universidade do Porto UPORTO, Portugal	PORTO FEUP FACULDADE DE ENGENHARIA UNIVERSIDADE DO PORTO
	Kungliga Tekniska Hoegskolan KTH, Sweden	KIH
	Universidad Politecnica de Madrid UPM, Spain	POLITECNICA
Beneficiaries	Bundesanstalt für Materialforschung und -Prüfung BAM, Germany	BAM Bundesanstalt for hater elder schang und -pollung
	Deutsche Bahn InfraGO AG DB, Germany	DB InfraGO
	Acoustique Et Vibrations Logiciels Scientifiques AVLS, France	AVLS
	Universitat Politecnica de Valencia UPV, Spain	UNIVERSITAT POLITÈCNICA DE VALÈNCIA
Affiliated	Universitat Jaume I de Castellon UJI, Spain	UNIVERSITAT JAUME I
Partners (to UPM)	Universidad de Sevilla UdS, Spain	Section of the sectio
	Administrador de Infraestructuras Ferroviarias ADIF, Spain	And odif
Associated Partner	University Of Huddersfield HUD, UK	University of HUDDERSFIELD Inspiring global professionals





<u>Acknowledgments:</u> This project has received funding from the Europe's Rail Joint Undertaking under Horizon Europe research and innovation programme under grant agreement No. 101121765 (HORIZON-ER-JU-2022-ExplR-02).

<u>Disclaimer:</u> Views and opinions expressed are however those of the author(s) only and do not necessarily reflect those of the European Union or Europe's Rail Joint Undertaking. Neither the European Union nor the granting authority can be held responsible for them.



TABLE OF CONTENTS

P	roject	co	nsortium	2
1		In	troductory remarks	4
2		M	ethodology	5
	2.1		Derailment criteria	5
	2.2		Parametric analysis	5
	2.3		Additional analysis	6
3		Nι	umerical modelling	6
	3.1		Bridge models	6
	3.2		Train models	. 10
	3.3		Rail irregularity profiles	. 15
4		Si	mulation setup	. 16
	4.1		Train-Track-Bridge Interaction.	. 16
	4.2		Selection of the critical HSLM-A	. 19
5		Si	mulation results	. 21
	5.1		Parametric analyses	. 21
	5.2		Additional analysis	. 26
	5.2	2.1	Influence of increased irregularities	. 26
	5.2	2.2	Influence of the bridge vibration	. 27
	5.2	2.3	Effect on riding comfort	. 28
6		No	ormative recommendation	. 31
	6.1		Concluding remarks	. 31
	6.2		Proposal for recommendation	. 32



1 INTRODUCTORY REMARKS

The current Eurocode EN 1990 (CEN, 2023b) uses deck acceleration as a criterion to ensure traffic safety on railway bridges. The norm limits vertical deck acceleration to 5.0 m/s² on ballastless bridges and to 3.5 m/s² on ballasted ones. Identical values can be found in the Chinese norm (National Railway Administration of the People's Republic of China, 2017), albeit the calculation of derailment indexes is often required (Montenegro et al., 2021). A different approach can be found in the Japanese norm (Railway Technical Research Institute, 2006), where safety is assessed by limiting deflection according to the number of spans, running speed, and track type.

While the Eurocode's limit for ballasted tracks is based on laboratory experiments (tests performed at the German Federal Institute for Materials Research and Training (BAM) in which the track instability occurred for accelerations from 7 m/s², commissioned by the European Rail Research Institute (ERRI D 214/RP 8, 1999) to validate the then European pre-standard (ENV)), the ballastless track limit is likely based on the assumption that a deck experiencing accelerations of 1 g implies that there may be loss of contact between wheel and rail. The lack of experimental or numerical proof supporting this value was noted by Zacher & Baeßler (2008) when replicating the BAM tests. Comparing these two values (7 m/s² and 1 g) to the limits inscribed in the norm, it seems like a safety factor equal to 2.0 was adopted to guarantee a safety margin. However, the validity of such a margin was not originally based upon a probabilistic method, which has led to the proposal of alternatives (Allahvirdizadeh et al., 2022) and studies that give a certain percentage allowance over the limit (Moliner et al., 2017).

The empirical link between deck acceleration and running safety has been addressed in preliminary studies. Using three-dimensional models (i.e. focusing solely on vertical dynamics), Arvidsson et al. (2018) found that deck accelerations reaching 1 g do not necessarily lead to wheel detachments; the fact that a point is subjected to 1 g acceleration does not imply the lifting of the entire train's mass. Since the mechanics that govern wheel-rail contact (and, by extension, the loss of contact and derailment) are complex and depend also on lateral components, the work presented in this report studies the risk of derailment considering three-dimensional advanced train—track—bridge interaction (TTBI) models with the purpose of comparing derailment criteria against calculated deck acceleration values to make a critical analysis of the traffic stability criteria stipulated in the EN 1990.

The core of the present study is a comparative analysis of deck acceleration and derailment criteria in five case study bridges (from 10 m to 30 m spans), considering two levels of track irregularities (high quality and alert limit) and running speeds from 150 km/h to 400 km/h. Considering the influence exerted by the track itself (Yang & Yau (2017) note that neglecting the rails can lead to an underestimation of results at high speeds) and the track's irregularities (Cai et al. (2016) connect its level with the derailment coefficient), additional analyses of increased irregularities and of the bridge vibration are presented. The connection between deck acceleration and riding comfort is also studied. The work presented in this report directly addresses the ERA technical note on work needed for closing TSI open point on bridge dynamics (European Union Agency for Railways, 2022) and includes results published by Ferreira et al. (2024).



2 METHODOLOGY

2.1 Derailment criteria

There are several criteria that can be used to assess train running safety, varying according to different derailment mechanisms and countries. These criteria (thoroughly summarized by Montenegro et al. (2021)) are based on the relation between the wheel-rail contact forces, which can only be accessed through TTBI models.

Among the available derailment criteria, the two used in this report (Nadal and Unloading) are among the most commonly used in the analysis of train running safety. The Nadal index ξ_N can be obtained through the following equation:

$$\xi_N = \frac{Y}{O} \tag{1}$$

where *Y* and *Q* are the time histories from the lateral and vertical contact forces, respectively, in each wheel. The Infrastructure TSI (European Commission, 2002) specifies a safety limit of 0.8 for this index.

Regarding the unloading index, ξ_U , it can be defined as:

$$\xi_U = 1 - \frac{Q}{Q_0} \tag{2}$$

where Q_0 is the wheel's static load. The criterion may also be analysed individually for each wheel. The European norm related to the testing and simulation of railway vehicles, EN 14363 (CEN, 2016), stipulates a limit of 0.6 for the unloading index. According to the same norm, before computing the aforementioned derailment criteria, the time histories of both vertical and lateral contact forces should be low-pass filtered with a cut-off frequency of 20 Hz using a filter of order 4. In this work, a Butterworth filter is adopted. Henceforth, the limits for the Nadal and Unloading criteria, as well as the acceleration limit, are referred to respectively as N_{lim} , U_{lim} , and a_{lim} .

2.2 Parametric analysis

The methodology employed involves conducting a parametric study on a set of 5 single-track slab bridges with spans ranging between 10 m and 30 m, with trains running at speeds ranging between 150 km/h and 400 km/h. For each analysis, the maximum values of the derailment indicators (Unloading and Nadal) and the maximum deck acceleration at midspan are recorded. Each bridge is paired with 1 out of 10 possible HSLM-A universal trains, i.e. only the most critical HSLM-A train for each bridge (the train that conditions the bridge design in terms of deck acceleration in the speed range) is considered in the analysis.

To study the effect of track irregularities, each bridge is simulated with a finite number of realizations of irregularity profiles, corresponding to a smooth track, a high-quality track, and an Alert Limit track. Therefore, the parametric study amounts to a total of 1430 3D TTBI dynamic simulations conducted using the numerical tool developed and validated by Montenegro et al. (2015). This number corresponds to the 5 bridges being tested with 11 different irregularities profiles (5 realizations of a higher quality track, 5 of lower quality track and 1 smooth track profile) with trains running at 26 possible speed values (10 km/h intervals of the speed range).



2.3 Additional analysis

This report is complemented by a study of 10 additional profiles where the track irregularities are increased above the normative Alert Limit, and with the study of a rigid bridge, to address the effects caused by the structure's vibration. Lastly, a study of whether deck acceleration can be considered an indicator of riding comfort is also presented.

3 NUMERICAL MODELLING

3.1 Bridge models

The characteristics of the bridges used for the present chapter were obtained from the work by Arvidsson and Andersson (2017) where, for simply supported single-span slab bridges, five models are proposed, with spans ranging from 10 m to 30 m and cross-sections designed to provide results near the Eurocode's acceleration limit when considering a design speed of 320 km/h (and consequently a maximum speed of 1.2×320 km/h, as per the EN 1991-2 (CEN, 2023a)).

For this work, the cross-sectional dimensions were obtained considering an elasticity modulus of 34 GPa and a Poisson's ratio of 0.2. The 3D models were developed with the Finite Elements Method using the commercial software ANSYS® (2018), using the following element types:

- BEAM188: Timoshenko beam elements to model the deck, the track slab and the rails;
- COMBIN14: spring-dashpots to model the track elements, namely the mortar bed between the deck and the track slab, the subgrade bed in the adjacent track to the bridge and the rail fastenings.

The bridge deck is modelled with beam elements located at its centre of gravity. From there, the track slab (which is also comprised of beam elements) is connected with an array of spring-dashpot elements that discretize the concrete-asphalt (CA) mortar bed. Above the slab, pairs of rigid elements reach the transversal coordinates of the rails, connecting to them through spring-dashpot elements that represent the fasteners and pads. The track slab is made up of modular sections with gaps at the abutments.

The properties of these bridges are presented in Table 1, including the span L, linear mass m, stiffness EI, the natural frequency of the first bending mode n_0 , cross-sectional width b,height h, and a slenderness ratio given by GAL^2/EI . Damping is accounted for through the use of a Rayleigh proportional matrix with damping ratios (taken from EN 1991-2 for all cases) set to the first two vertical bending modes of the bridge deck.

Slenderness h(m)L(m)m (ton/m)EI (GN m^2) n_0 (Hz) b (m)ratio 10 12.5 14.3 15.4 8.15 0.64 481.9 21.2 9.2 7.31 15 36 1.03 1136.5 20 25.4 65.1 6.4 7.01 1.32 2061.1 25 33.1 152.0 6.72 3295.2 5.4 1.83 36.7 4.2 30 211.0 6.63 2.07 4779.8

Table 1: Properties of the bridge models.



Regarding the track elements, their vertical mechanical properties (stiffness and damping) were adopted from Arvidsson et al. (2018), while the lateral and longitudinal characteristics were adopted from the 3D TTBI models developed by Montenegro et al. (2020), (2022) and Neto et al. (2021). The properties of the slabs and UIC60 rails with 1.435 m gauge (density ρ , modulus of elasticity E, area A, moment of inertia I, height h and width b) are listed in

Table 2. The properties of the fasteners and elastic bed, adapted from Arvidsson et al. (2018), ERRI D 214/RP 11 (1997), Ling et al. (2019), and Shi et al. (2016), are listed in Table 3 and in Table 4, where *x*, *y*, and *z* indicate the longitudinal, transversal, and vertical directions, respectively.

Table 2: Properties of the slabs and rails.

	ρ (kg/m ³)	E (GPa)	A (m ²)	$I(\mathrm{m}^4)$	h (m)	<i>b</i> (m)
Slabs	2400	34	0.96	7.2×10 ⁻³	0.3	3.2
Rails	7850	210	7.676×10 ⁻³	30.038×10 ⁻⁶	-	-

Table 3: Properties of the fasteners.

	stiffness (MN/m)	damping (kNs/m)	rotational stiffness (kN m/rad)	Spacing (m)
Longitudinal	40	40	45	
Transversal	40	40	45	0.588
Vertical	22.4	5.47	45	•

Table 4: Properties of the elastic bed.

	Modulus (MN/m ³)	Damping (kNs/m²)
Mortar	1×105	34.58
Subgrade	100	34.58

A transversal schematic representation of the FE models is shown in Figure 1, and its lateral counterpart is shown in Figure 2. A characteristic 3D view of the ANSYS® model. While the deck and track slab's properties can be reduced to single beams to enable the coupling of a three-dimensional vehicle model, each rail must be modelled separately, thus justifying the configuration of rigid elements that can be seen in the same figure. Lastly, each bridge's first vertical bending modal shapes and frequencies can be seen in Figure 4.



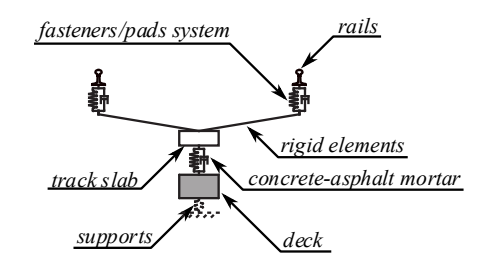


Figure 1: Transversal schematic representation of the bridge models.

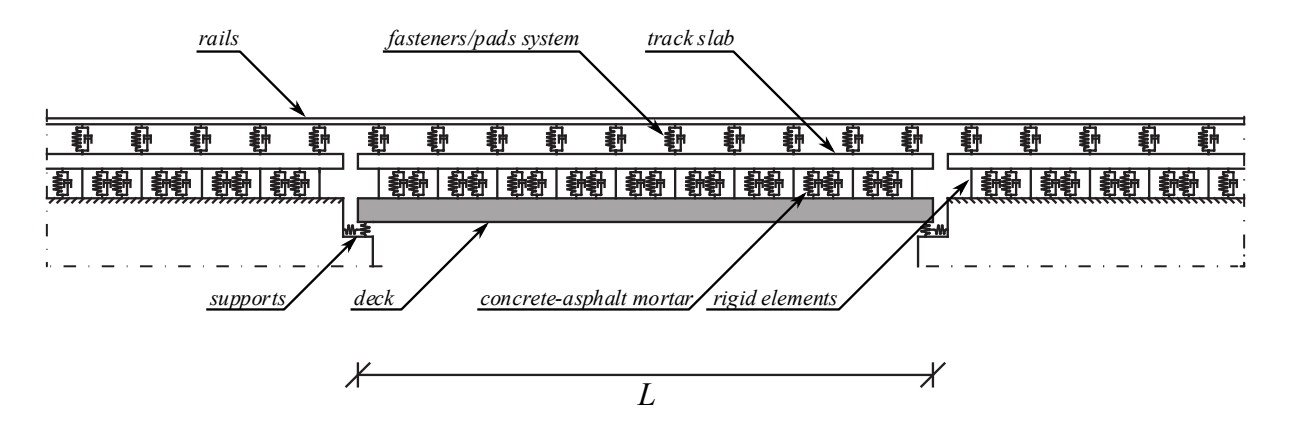


Figure 2: Lateral schematic representation of the bridge models.

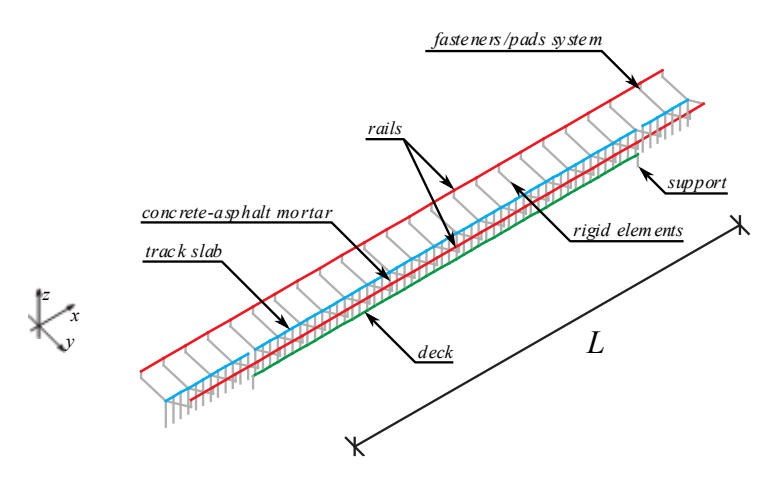


Figure 3: View of the typical FE bridge model.



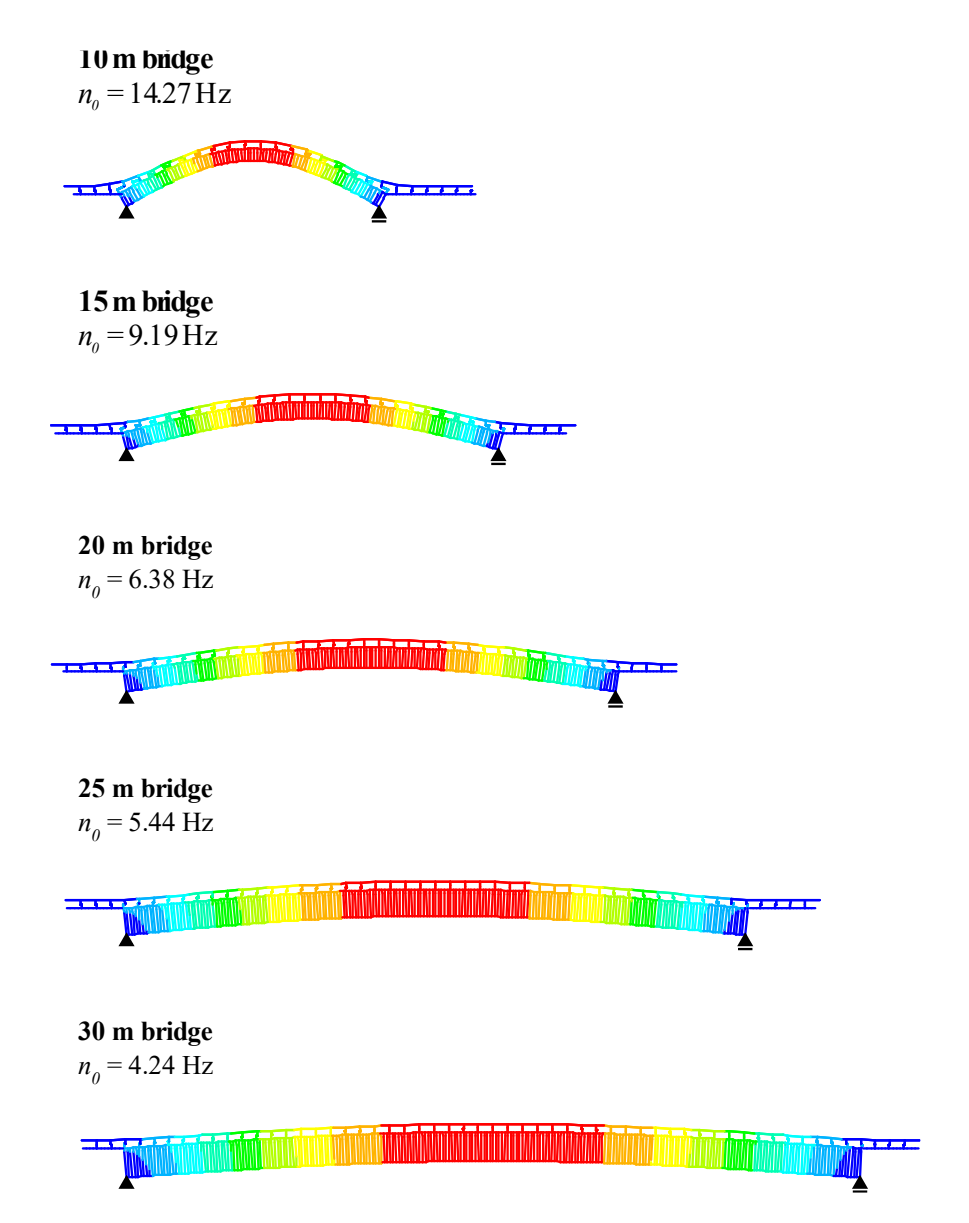


Figure 4: First vertical bending modes of the FE ballastless track bridge models.



3.2 Train models

The train models used for loading in this report are 3D vehicles aimed to represent the High-Speed Load Model A (HSLM-A). This approach was selected since the HSLM envelope is intended to cover a wide range of possible running trains. The HSLM-A is a moving load model specified in EN 1991-2, which includes axle distances and loads with a geometric configuration resembling articulated trains, without any explicit suspension or vehicle body data provided by the norm. Therefore, the relevant information regarding the vertical dynamic behaviour was retrieved from Arvidsson et al. (2018), for each of the 10 HSLM-A trains. The authors of that study adjusted the car body masses to correspond to the axle loads (ranging from 17 to 21 tonnes/axle) and the characteristics of the primary and secondary suspensions to produce realistic bounce frequencies. In contrast, the lateral and longitudinal suspensions were adopted from typical three-dimensional trains found in the literature (Goicolea, 2014; Lee & Kim, 2010). Table 5 lists the symbols used to describe the train model parameters. A thorough list of the values can be consulted in Tables 6, 7, 8, 9, and 10.

Table 5: Train model parameter symbols

Table 3. Train model parameter symbols.					
Mechanical properties					
	Moments of inertia				
	Mass Roll Pitch Yaw				
Car body	m_{cb}	$I_{cb,x}$	$I_{cb,y}$	$I_{cb,z}$	
Bogie	m_b	$I_{b,x}$	$I_{b,y}$	$I_{b,z}$	
Wheelset	m_w	$I_{w,x}$	-	$I_{w,z}$	
	Susp	ension prope	erties		
Direction					
		x	у	Z	
Stiffness k k k					



Table 6: Parameters of the train models (intermediate coaches).

HSLM train	m_{cb} (kg)	$I_{cb,y}$ (kg m ²)	$I_{b,y}$ (kg m ²)
A1	27160	0.91×10 ⁶	1240
A2	33280	1.41×10^{6}	3650
A3	29200	1.19×10 ⁶	1240
A4	31240	1.51×10 ⁶	2700
A5	27160	1.31×10 ⁶	1240
A6	29200	1.53×10^6	1240
A7	31240	1.77×10^{6}	1240
A8	31240	1.98×10 ⁶	1900
A9	35310	2.32×10 ⁶	1240
A10	35310	2.49×10 ⁶	1240

Table 7: Parameters of the train models (end coaches).

HSLM train	m_{cb} (kg)	$I_{cb,y}$ (kg m ²)	$I_{b,y}$ (kg m ²)
A1	40740	1.02×10^6	1240
A2	49910	1.52×10 ⁶	3650
A3	43800	1.37×10 ⁶	1240
A4	46850	1.69×10^6	2700
A5	40740	1.54×10 ⁶	1240
A6	43800	1.82×10 ⁶	1240
A7	46850	2.12×10 ⁶	1240
A8	46850	2.36×10^6	1900
A9	52970	2.83×10^{6}	1240
A10	52970	3.06×10^6	1240



Table 8: Parameters of the train models (power cars).

HSLM train	m_{cb} (kg)	$I_{cb,y}$ (kg m ²)	$I_{b,y}$ (kg m ²)
A1	54320	1.33×10^6	2700
A2	66550	1.62×10^6	2700
A3	58400	1.43×10 ⁶	2700
A4	62470	1.53×10 ⁶	2700
A5	54320	1.33×10 ⁶	2700
A6	58400	1.43×10 ⁶	2700
A7	62470	1.53×10 ⁶	2700
A8	62470	1.53×10^6	2700
A9	70630	1.72×10^6	2700
A10	70630	1.72×10 ⁶	2700

Table 9: Varying parameters of the train models (all coaches).

HSLM train	$k_{p,z}$ (kN m)	$c_{p,z}$ (kN m/s)	$k_{s,z}$ (kN m)	$c_{s,z}$ (kN m/s)
A1	1410	20	640	39
A2	1320	19	820	50
A3	1380	20	700	43
A4	1350	19	760	46
A5	1410	20	640	39
A6	1380	20	700	43
A7	1350	19	760	46
A8	1350	19	760	46
A9	1280	19	880	53
A10	1280	19	880	53



Parameter	Unit	Value
$I_{cb,x}$	kg m ²	119,328
$I_{cb,z}$	kg m ²	1,957,888
m_b	kg	3,500
$I_{b,x}$	kg m ²	2,835
$I_{b,z}$	kg m ²	4,235
$m_{\scriptscriptstyle \mathcal{W}}$	kg	2,000
$I_{w,x}$	kg m ²	1,000
$I_{w,z}$	kg m ²	1,000
$k_{p,x}$	kN m	12,500
$k_{p,y}$	kN m	120,000
$C_{p,x}$	kN m/s	9
$C_{p,y}$	kN m/s	27.9
$k_{s,x}$	kN m	2,500
$k_{s,y}$	kN m	240
$C_{S,X}$	kN m/s	30
$C_{S,y}$	kN m/s	30

Table 10: Common parameters of the train models (all coaches).

The 3D FE models were developed in the ANSYS® commercial software, using three of its available finite element types:

- BEAM4: 3D elastic beams, to act as rigid beams;
- MASS21: 3D structural mass, to model all localized masses and rotational moments of inertia.

Each wheelset is connected to a primary suspension linked to the bogie via rigid beams. The bogies are connected to a secondary suspension that, in turn, is linked to the geometric centre of the car body. The HSLM is characteristically comprised of a power car at each end (with two bogies, independent of the rest of the train), an end coach attached to each power car (with an independent bogie and a shared bogie) and a succession of intermediate coaches that share bogies in the manner of an articulated train. The load model is symmetrical; therefore, the last intermediate coach shares a bogie with another end coach, which is followed by the final power car.

It is highlighted that the HSLM is a load model and not an actual train, presenting the challenge of articulating the intermediate coaches in the FE model. For this work, the solution achieved was to connect the secondary suspension to one of the carriages and then to couple the translational degrees of freedom of that suspension with those of the following carriage, allowing for free rotation in every axis, effectively modelling a spherical joint. This approach is sufficient to analyse lateral and vertical forces at the level of the wheels, which is the intended purpose of the study. Figure 5 depicts lateral and front views of a schematic representation of the train model, while the corresponding FEM implementation can be seen in Figure 6.



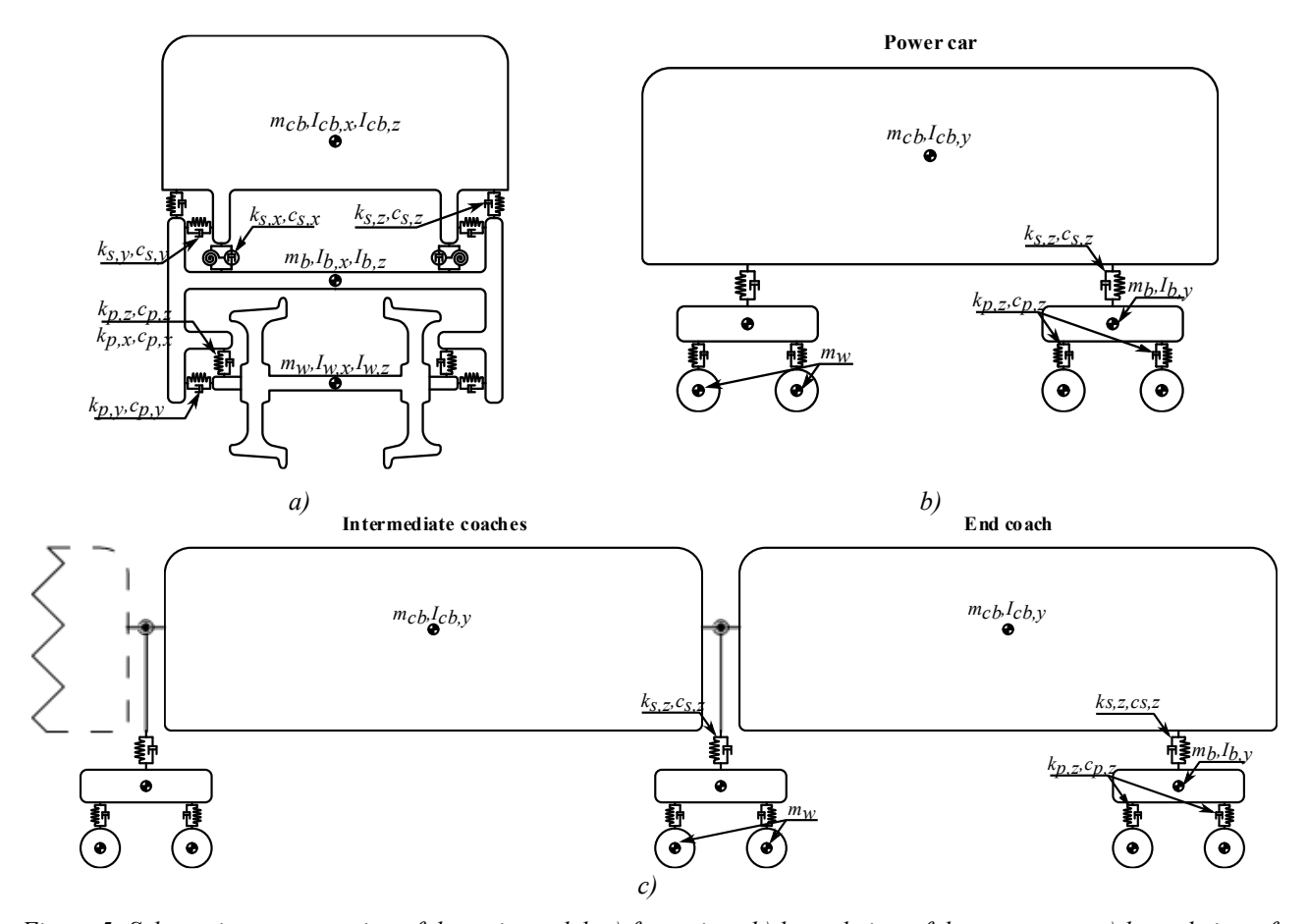


Figure 5: Schematic representation of the train model. a) front view; b) lateral view of the power car; c) lateral view of the end and intermediate coaches.

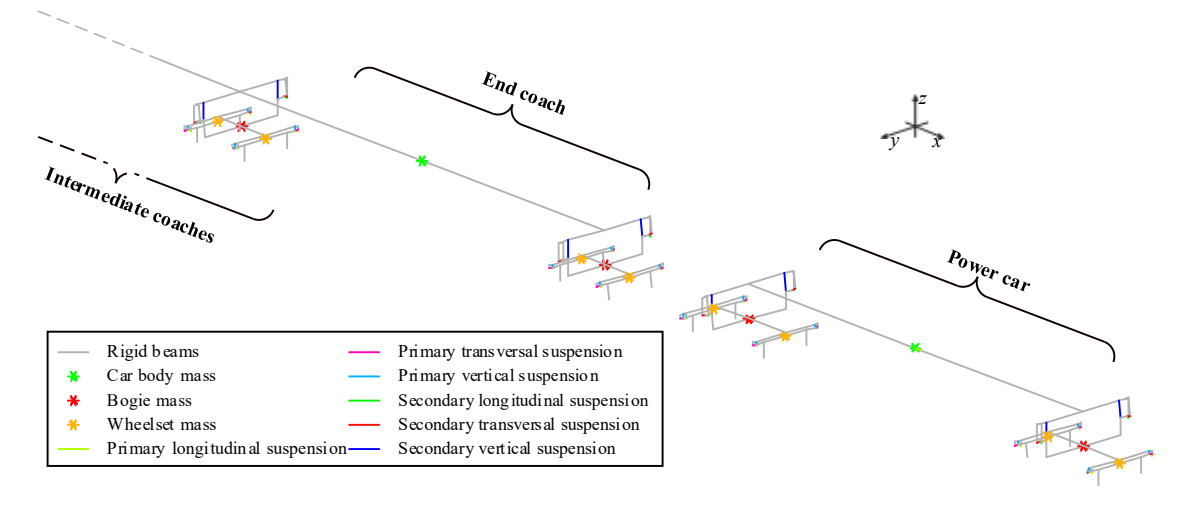


Figure 6: View of the train's FEM model.



3.3 Rail irregularity profiles

The track irregularity profiles employed in the present work were artificially generated based on the German Power Spectral Density (PSD) functions procedure described by Claus & Schiehlen (1998), where the irregularities r along the longitudinal development x are given by:

$$r(x) = \sqrt{2} \sum_{n=0}^{N-1} A_n \cos(\Omega_n x + \varphi_n)$$
 (3)

where N is the number of frequencies (Ω_n) , φ_n is a random phase angle between 0 and 2π , and A_n are factors given by the same study.

The wavelength interval 3-150 m was considered for generating the profiles, which includes the D1 (3-25 m), D2 (25-70 m), and D3 (70-150 m) ranges specified in the EN 13848-5 (CEN, 2015). Two track quality levels were considered:

- Lower track quality: with track quality factors for longitudinal (vertical) and alignment levels of $A_v = 6.00 \times 10^{-7}$ and $A_a = 2.70 \times 10^{-7}$, to obtain standard deviations in the D1 range compatible with the Alert Limit specified in the EN 13848-5 for speeds up to 300 km/h of $\sigma_{3-25,v}$ equal to 1.25 mm and $\sigma_{3-25,a}$ of 0.85 mm for the longitudinal and alignment profiles, respectively;
- Higher track quality: with track quality factors of $A_v = 0.60 \times 10^{-7}$ and $A_a = 0.35 \times 10^{-7}$, respectively, giving $\sigma_{3-25,v}$ equal to 0.40 mm and $\sigma_{3-25,a}$ of 0.30 mm, compatible with a well-maintained track of the Chinese PSD (Zhai et al., 2015).

Plots of example realizations of tracks' irregularities can be seen in Figure 7 and Figure 8 for higher and lower quality, respectively. An example of the alignment PSD is shown in Figure 9.

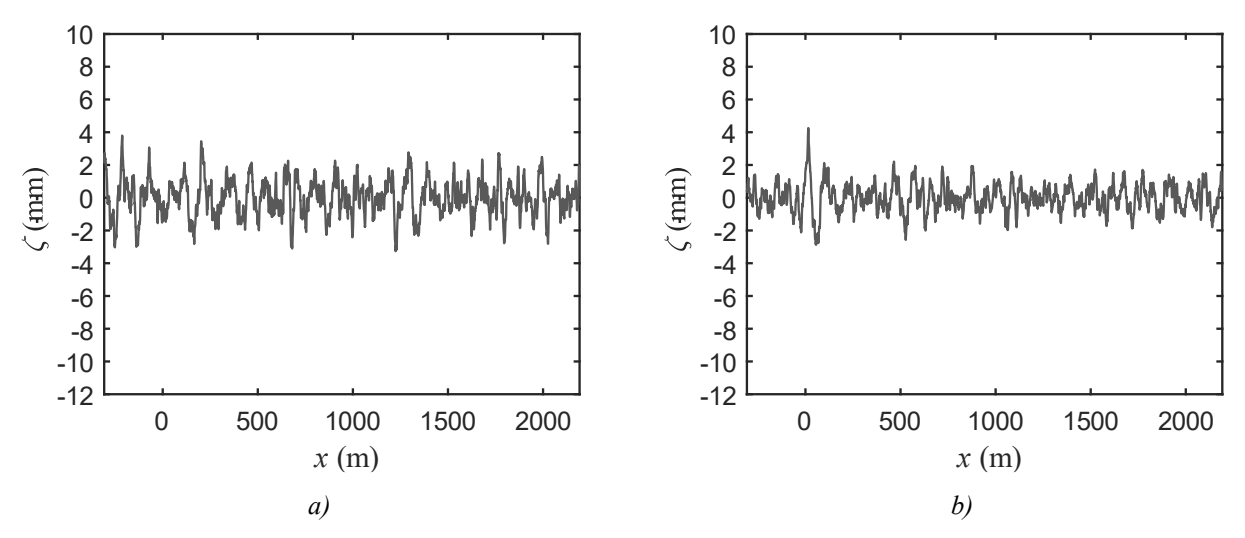


Figure 7: Example realization of a higher quality track irregularity profile. a) vertical direction; b) lateral direction.



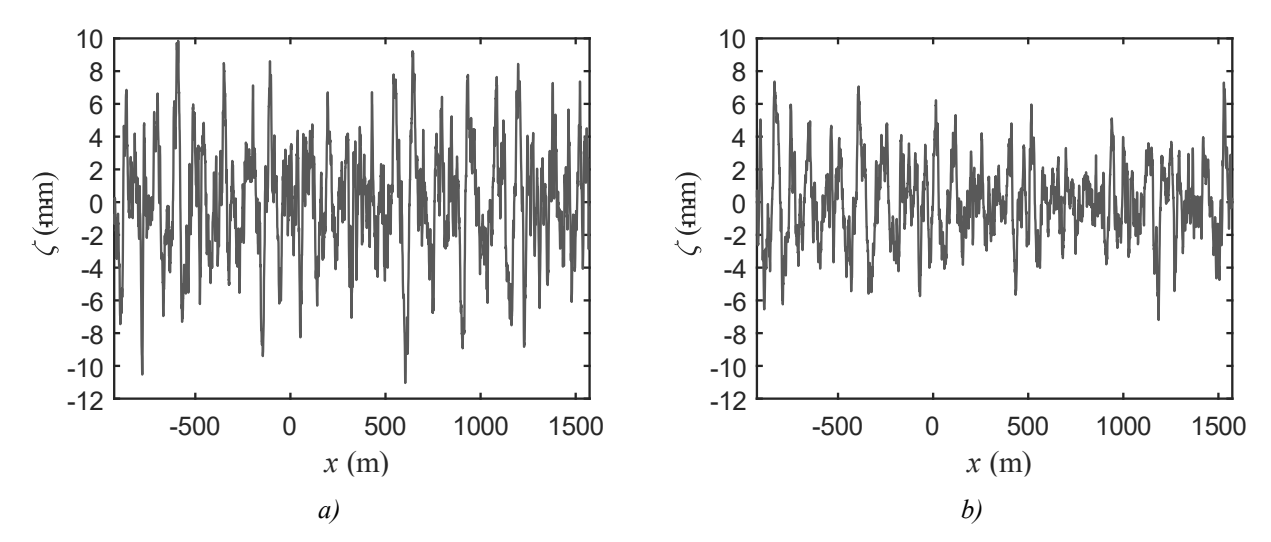


Figure 8: Example realization of a lower quality track irregularity profile. a) vertical direction; b) lateral direction.

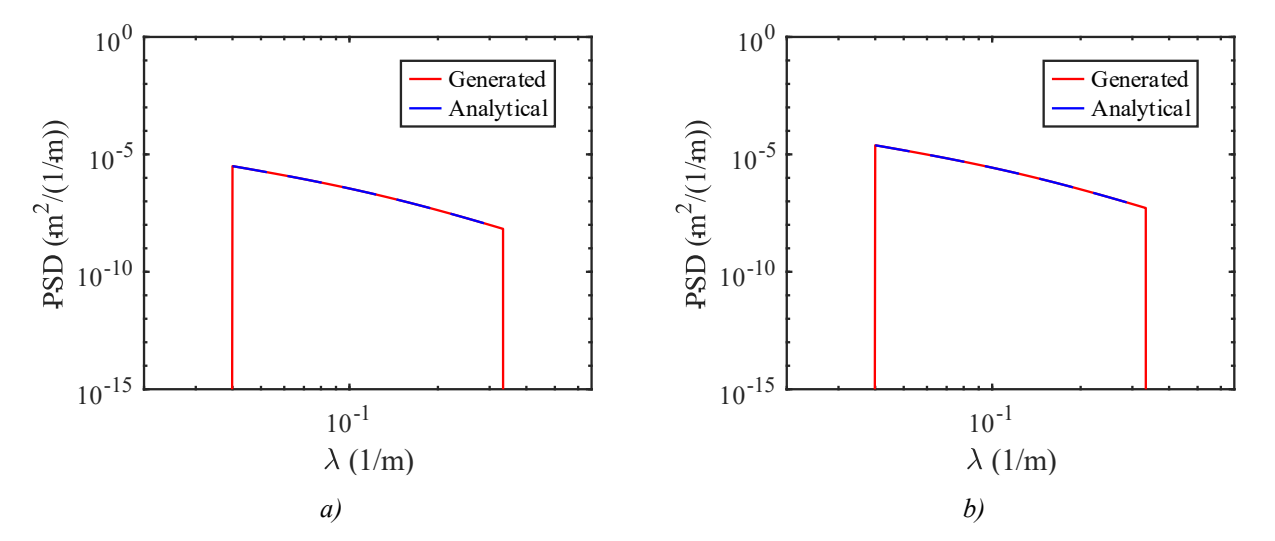


Figure 9: Example PSD of the alignment irregularities. a) well-maintained track; b) Alert limit.

4 SIMULATION SETUP

4.1 Train-Track-Bridge Interaction

The 3D TTBI dynamic analyses are carried out using the software "VSI — Vehicle Structure Interaction Analysis", whose application for this report is illustrated in Figure 10. This tool, capable of dealing with lateral dynamics, is implemented in MATLAB® (2018) and imports the structural matrices from the railway vehicle and bridge modelled in ANSYS®. The external excitations are imposed on the coupling system, and the corresponding dynamic responses are obtained. The interaction between the two sub-systems is accomplished by a specially developed contact finite element that considers the behaviour of the contact interface between wheel and rail. The contact formulation is divided into three parts: the geometrical, normal and tangential contact problems. With the contact interface fully characterized, the equations of motion of the vehicle and bridge are complemented with constraint equations that couple these two structural systems. The full mathematical formulation and validation of the TTBI procedure can be found in Neves et al. (2014) and in Montenegro et al. (2015).



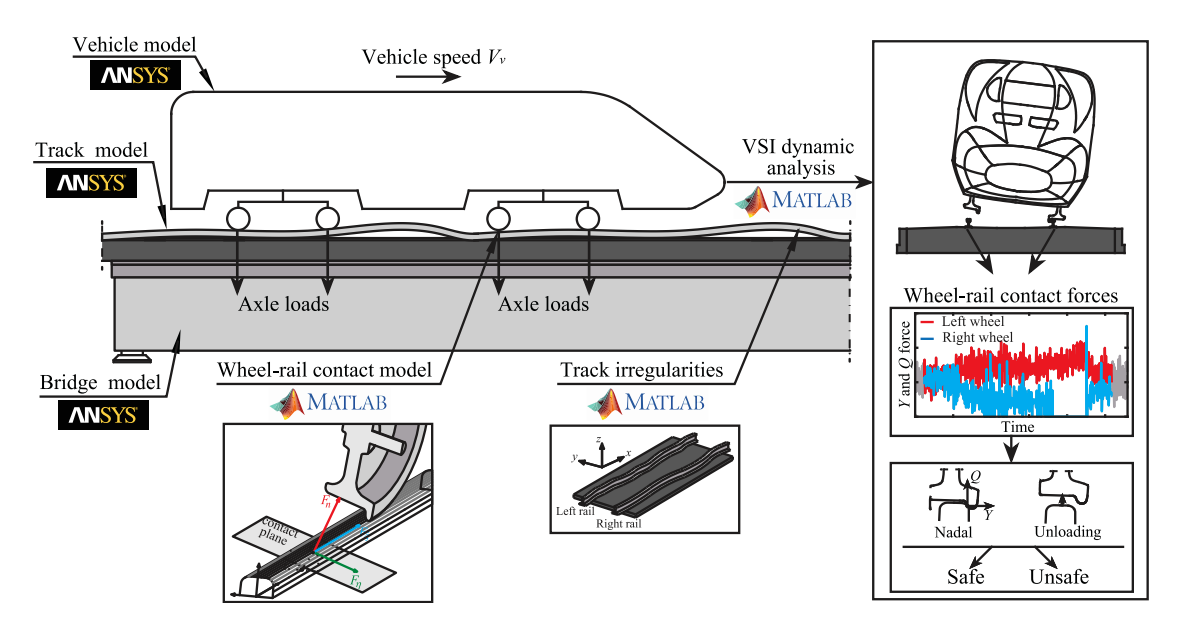


Figure 10: Framework of the tool for 3D TTBI dynamic analysis.

The wheel-rail contact formulation relies on a contact finite element specially developed for the TTBI numerical tool. This element, implemented in MATLAB®, is first used to evaluate the location of the contact point between wheel and rail based on the relative movement between the vehicle and the structure. This first step, called the geometrical contact problem, is accomplished with the parameterization of the surfaces of the contacting bodies, namely the wheel and rail. The potential contact point position is evaluated through the following nonlinear equations:

$$\begin{cases} \mathbf{t}_r \cdot \mathbf{d}_{wr} = 0 \\ \mathbf{t}_w \cdot \mathbf{n}_r = 0 \end{cases} \tag{4}$$

where \mathbf{t}_r and \mathbf{t}_w are the lateral tangent vectors to the rail and wheel surfaces, respectively, at the contact point, \mathbf{n}_r is the normal vector to the rail surface at that same point and \mathbf{d}_{wr} is the vector defining the relative position between the contact points in the wheel and rail surfaces pointing towards the wheel. However, as it can be seen in Figure 11, the condition defined by Eq. (4) is necessary but not sufficient to guarantee an actual contact. Therefore, the following additional condition is added to the formulation to ensure that the two parametric surfaces intersect each other:

$$\mathbf{d}_{wr} \cdot \mathbf{n}_r \le 0 \tag{5}$$

Since \mathbf{d}_{wr} points towards the wheel and the normal vector \mathbf{n}_r points outside the rail surface, Eq. (5) represents the situation A illustrated in Figure 11, in which contact occurs when the two vectors point in opposite directions. If this condition is not met, although the solution for Eq. (4) is valid, no contact occurs, as shown in situation B depicted in Figure 11. The deformation of the contact element, which is used to calculate the normal contact force, is given by:

$$d = \|\mathbf{d}_{wr}\| \tag{6}$$

For a better and faster convergence, the results obtained in the previous iteration or step are used as an initial estimate for the solution of the nonlinear problem defined through Eq. (4). Note that the system of equations (4) may have multiple solutions if the contact point falls in the concave region between the wheel



thread and flange. When this occurs, an alternative contact point detection algorithm, described in detail by Montenegro et al. (2015), is employed.

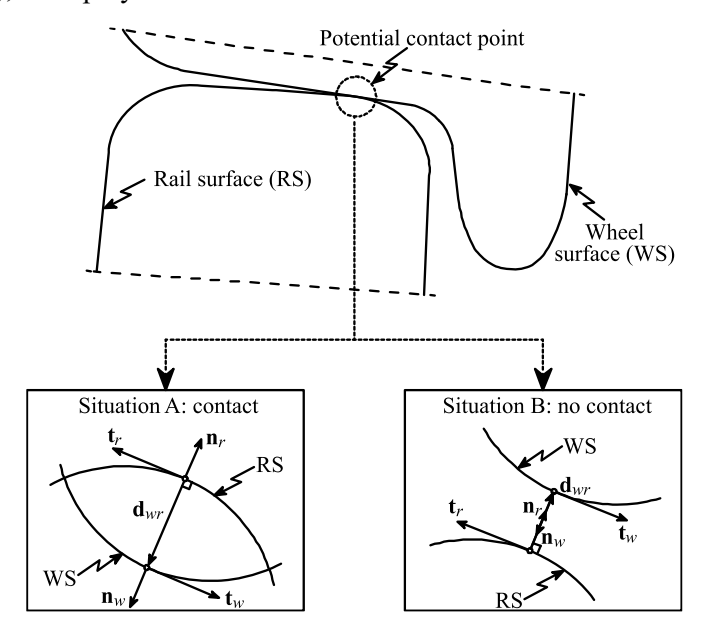


Figure 11: Possible scenarios that arise from a valid solution of the nonlinear equations for contact search.

The forces that arise in the contact interface are evaluated through the contact laws implemented in the contact finite element. Regarding the normal contact, and according to the Hertz nonlinear theory, when two non-conforming bodies are compressed against each other, they deform in the region around the first contacting point, forming a contact patch with an elliptical format. The normal contact force F_n can thus be computed based on the deformation d of the contact element calculated in Eq. (6) through the following equation:

$$F_n = K_h d^{\frac{3}{2}} \tag{7}$$

where K_h is a coefficient depending on the Young's modulus and Poisson ratio of the material from the contacting bodies and on their curvatures at the contact point.

After computing the normal forces, it is possible to evaluate the tangential forces that arise on the contact interface due to the rolling friction contact between the wheel and rail. Contrary to the Coulomb friction, where the behaviour within the contact patch is homogeneous (all points are adhering or slipping), when two compressing bodies are allowed to roll over each other, the contact area may share points in adhesion and in slippage simultaneously. Based on this, it is possible to compute the so-called creepages, which consist of the normalized relative velocities between the wheel and rail at the contact point. These creepages are the primary inputs for the tangential contact forces, which play a major role in the vehicle's stability. The tangential creep forces in the longitudinal, F_{ζ} , and lateral, F_{η} , directions (see Figure 12), are precalculated and stored in a lookup table, based on the USETAB algorithm (Kalker, 1996), to be later interpolated during the dynamic analysis as a function of the creepages and the semi-axes ratio of the contact ellipse (see Montenegro et al. (2015) for details about how the table was built).



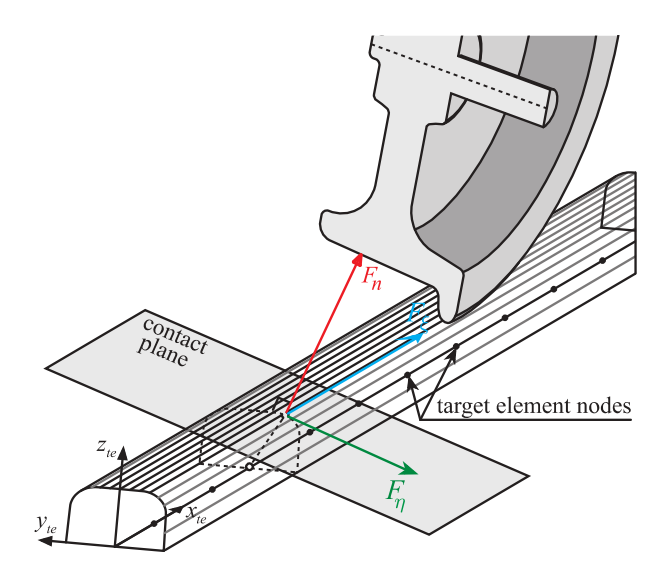


Figure 12: Normal and tangential contact forces in the contact interface between wheel and rail.

The coupling between the vehicle and the bridge is accomplished through the Lagrange multipliers method, in which the governing equilibrium equations of motion are complemented with constraint equations that connect the two sub-systems. These equations form a single system with displacements $\bf a$ and contact forces $\bf X$ (Lagrange multipliers) as unknowns that can be mathematically described as

$$\begin{bmatrix} \overline{\mathbf{K}} & \overline{\mathbf{D}} \\ \overline{\mathbf{H}} & \mathbf{0} \end{bmatrix} \begin{bmatrix} \Delta \mathbf{a}^{i+1} \\ \Delta \mathbf{X}^{i+1} \end{bmatrix} = \begin{bmatrix} \mathbf{\Psi} \left(\mathbf{a}^{t+\Delta t,i}, \mathbf{X}^{t+\Delta t,i} \right) \\ \overline{\mathbf{r}} \end{bmatrix}$$
(8)

where $\overline{\mathbf{K}}$ is the coupled effective stiffness matrix of the system, and $\overline{\mathbf{r}}$ is the track irregularities vector that is interpolated in each timestep depending on the position of the wheel. Due to the nonlinear nature of the problem, a formulation based on incremental displacements $\Delta \mathbf{a}$ and contact forces $\Delta \mathbf{X}$ has been implemented, in which $\boldsymbol{\psi}$ is the residual force vector. Finally, since node B from the contact element is located over non-nodal points from the track (the contact element is constantly moving), matrix $\overline{\mathbf{D}}$ transforms the contact forces defined in the local coordinate system (CS) of the rail elements with the nodal forces in the global CS, while matrix $\overline{\mathbf{H}}$ relates the nodal displacements of the rail elements in the global CS with the displacements of the non-nodal points from the rail elements where node B is located. Superscript $t+\Delta t$ indicates the current time step, while i and i+1 refer to the previous and current iteration.

4.2 Selection of the critical HSLM-A

As mentioned, only the most critical HSLM-A train for each case study bridge is considered for the parametric study. A simple moving loads method, applicable to single-span simply supported bridges, was employed for this assessment, using the bridges' properties and the load values and distances of the HSLM-A.

The maximum midspan acceleration *a* is estimated while accounting for the resonant effects that occur due to the relation between the repeatability of the loads and the bridges' natural vibration frequencies. Each line of the graphics in Figure 13 corresponds to the maximum acceleration obtained from the response of each of the HSLM-A trains at different speeds on each bridge. The HSLM-A universal train (represented in blue) that causes an acceleration that exceeds the EN 1990 limit of 5 m/s² (at around 1.2×320 km/h) was chosen as the critical one for that bridge. Therefore, the critical HSLM-bridge pairs are: 10 m bridge with HSLM-A7; 15 m bridge with HSLM-A7; 20 m bridge with HSLM-A1; 25 m bridge with HSLM-A3; 30 m bridge with HSLM-A9.



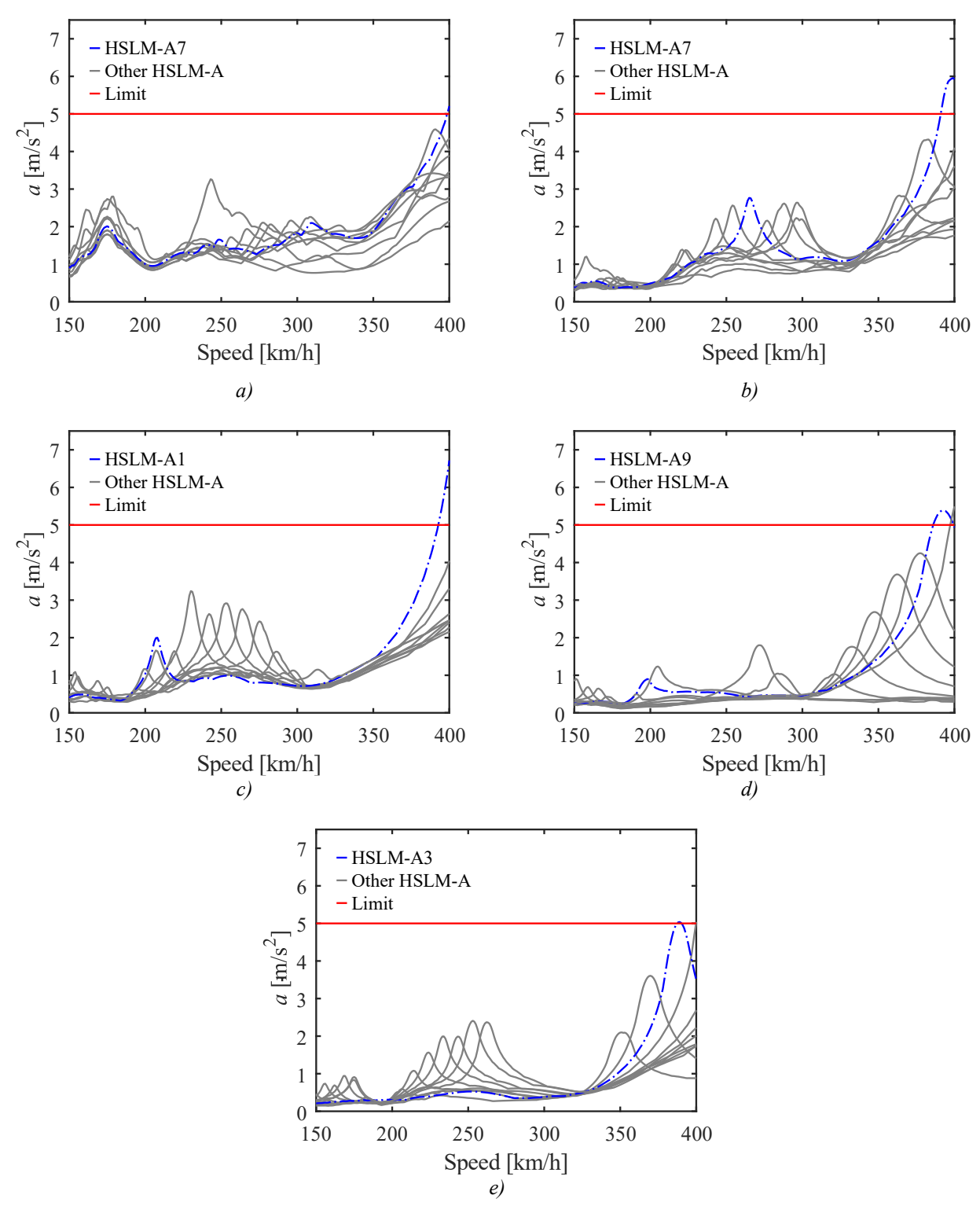


Figure 13: Maximum midspan deck acceleration and identification of the most critical HSLM-A train. a) 10 m bridge; b) 15 m bridge; c) 20 m bridge; d) 25 m bridge; e) 30 m bridge.



5 SIMULATION RESULTS

5.1 Parametric analyses

The results of the parametric analyses are presented hereinafter. Figure 14 depicts the envelopes of the maximum registered Unloading criteria, while the Nadal envelopes are presented in Figure 15. The displayed data points of the computed derailment criteria correspond, for each speed, to the worst-performing wheelset (while still on the bridge) of that particular simulation. The acceleration values can be seen in Figure 16, with each value representing the maximum absolute acceleration at the midspan of the bridge's deck.

The Nadal criterion measures no distinguishable features for a smooth track profile (i.e., with no vertical or lateral rail irregularities imposed on the system). Due to the absence of lateral irregularities and other sources of transversal instability, this behaviour is expected, serving as a benchmark for the results. In fact, the vertical acceleration curves for smooth tracks show similarities to the moving loads assessment in both absolute value and location of resonance.

Concerning the track irregularities, whether of high or low quality (Alert Limit level), the maximum values of ξ_U increase with speed, but the general shape of their trends remains the same (Figure 14). The same conclusion can be drawn from the results of the accelerations. Notably, the Unloading criterion curves rise as the speed approaches 400 km/h, but they also show a less evident, yet present, peak around the sub-harmonic speeds.

In general, it is observed that ζ_N is unaffected by resonance phenomena, never following the trend of the acceleration or Unloading curves but instead reflecting only the level of track condition (Figure 15). As the irregularities (including lateral) on the tracks become more prevalent, lateral forces become more prononuced in each wheel, while vertical contact forces get diminished, thus increasing the criterion's values. However, even in scenarios with low-quality tracks (characterized with Alert Limit irregularity profiles), the Nadal criterion remains fairly low and distant from its limit of 0.8

Table 12 for the Alert Limit irregularity profiles. Both tables present the two concomitant criteria, i.e., the maximum value of the worst-performing wheelset that stems from the realization of rail irregularity leading to the maximum acceleration. From the observation of these results, there appears to be no correlation between acceleration levels above the normative limit of 5 m/s² and derailment indicators. Considering, for example, the worst-case scenario of track condition, an assessment based on the normative limit would conclude that the acceleration limit is surpassed. However, the maximum value of the unloading factor, in that case (for all studied bridges), is below 0.38 for high-quality tracks and 0.48 for Alert Limit tracks, which is far from the limit of 0.6. Therefore, since deck acceleration does not seem to condition derailment at such low values, the results do not support the thesis of safety being limited by the calculation of vertical deck acceleration.



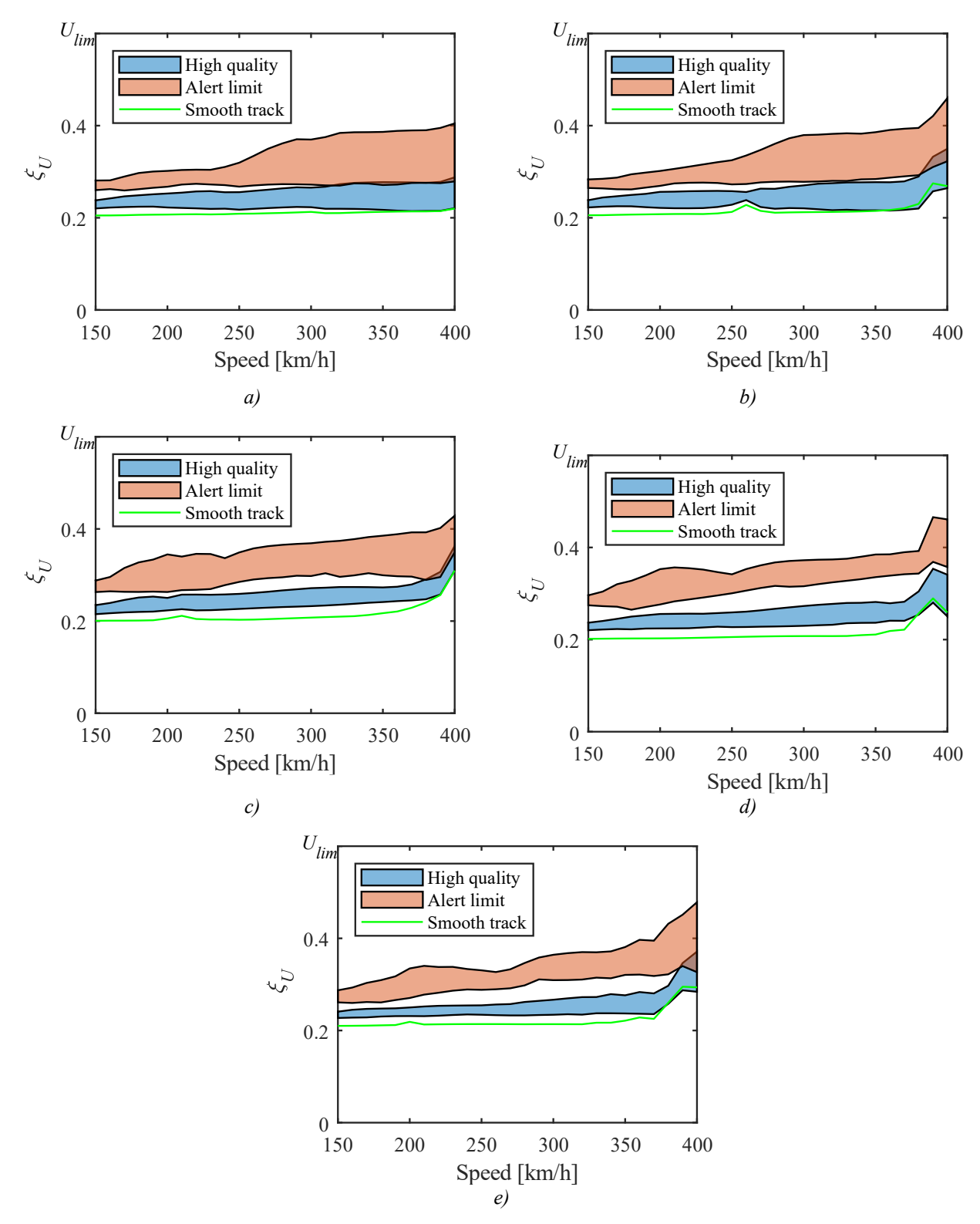


Figure 14: Unloading criterion envelopes. a) 10 m bridge; b) 15 m bridge; c) 20 m bridge; d) 25 m bridge; e) 30 m bridge.



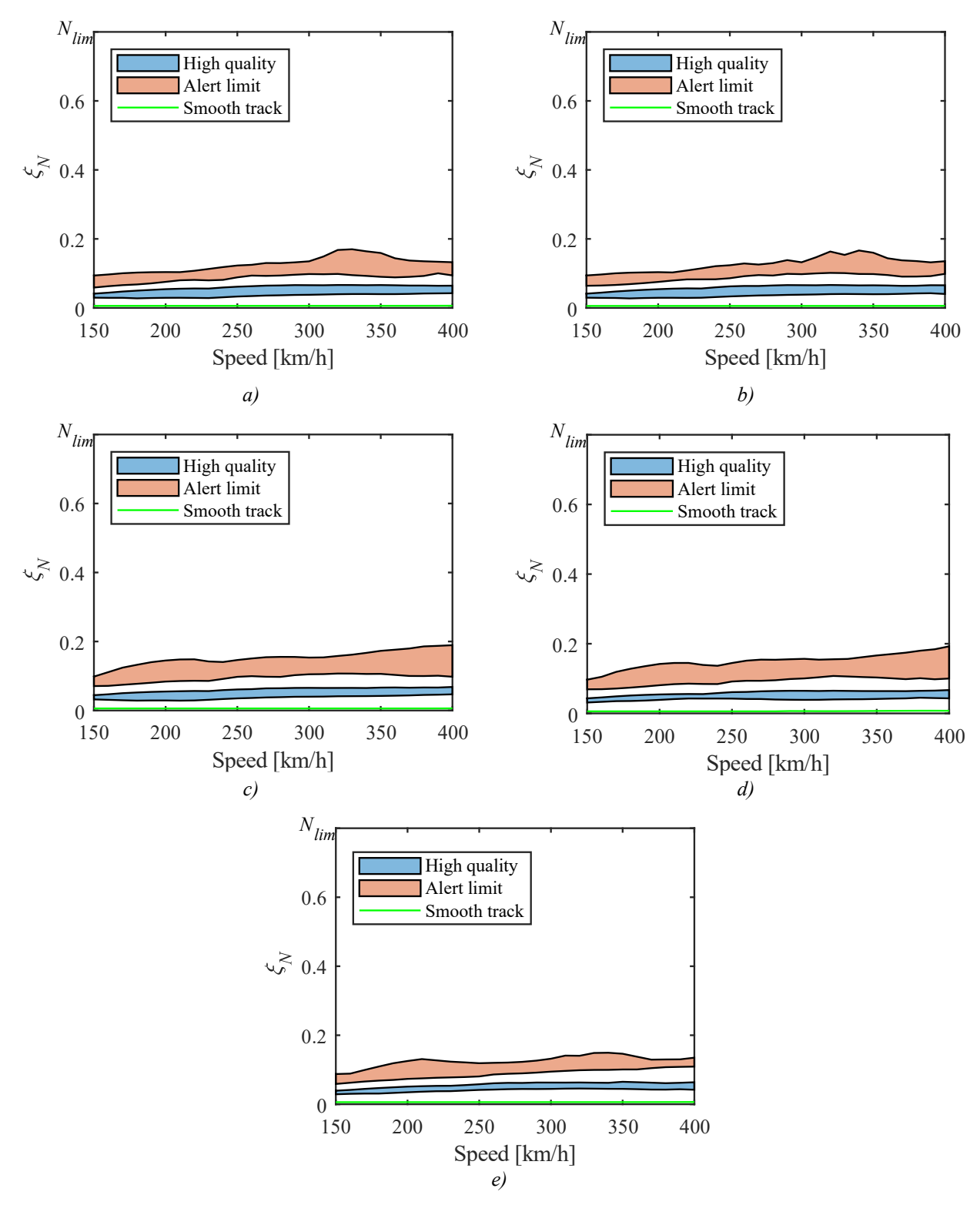


Figure 15: Nadal criterion envelopes. a) 10 m bridge; b) 15 m bridge; c) 20 m bridge; d) 25 m bridge; e) 30 m bridge.



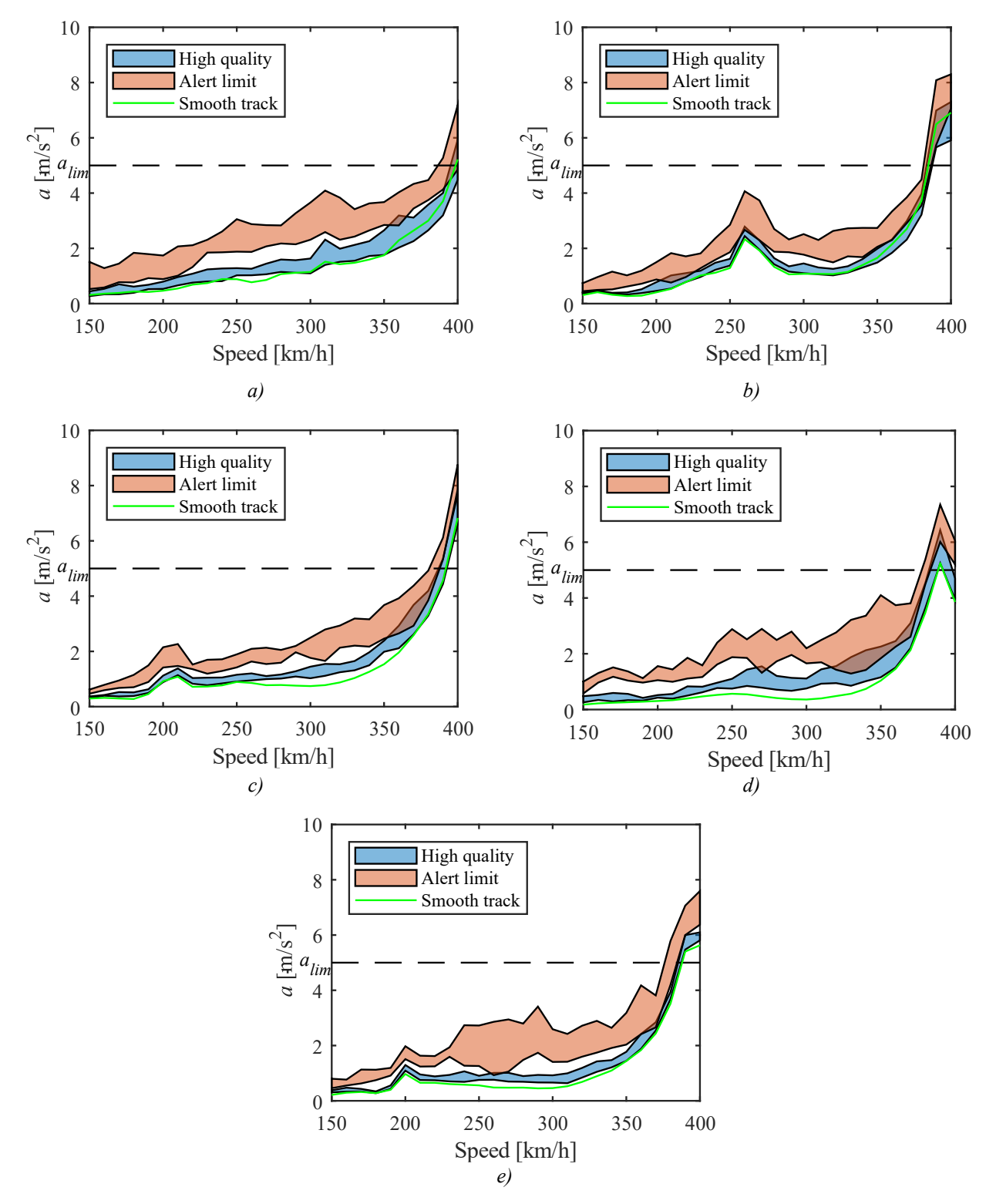


Figure 16: Vertical deck acceleration envelopes. a) 10 m bridge; b) 15 m bridge; c) 20 m bridge; d) 25 m bridge; e) 30 m bridge.



30 m

		Criteria	
Bridge	Max. accel. (m/s ²)	Unloading	Nadal
10 m	5.93	0.25	0.04
15 m	7.30	0.26	0.07
20 m	7.70	0.36	0.07
25 m	6.43	0.30	0.06

Table 11: Maximum registered acceleration values and concomitant criteria (high-quality track).

Table 12: Maximum registered acceleration values and concomitant criteria (Alert Limit track).

0.29

0.06

6.09

		Criteria	
Bridge	Max. accel. (m/s ²)	Unloading	Nadal
10 m	7.18	0.28	0.10
15 m	8.30	0.38	0.13
20 m	8.77	0.39	0.10
25 m	7.35	0.37	0.12
30 m	7.59	0.36	0.11

The existence of a correlation (or lack thereof) between acceleration and derailment indicators can be further explored by plotting all the pairs of data points and fitting a linear regression, as seen in Figure 17, where the continuous black lines represent the fitted models. The displayed coefficients of determination (r^2) show, for both cases, that the Unloading criterion is the one that follows acceleration the closest. Even so, the relation is insufficient to infer safety conditions from analysing acceleration alone, since several data points above the acceleration limit do not cross U_{lim} . This observation is even more evident when considering lateral forces for derailment, i.e. acceleration values from close to 0 m/s² to almost 8 m/s² hardly translate into any relevant ξ_N values. It is also worth noting that the gap between the criteria's r^2 values is narrower for the worst track conditions, which highlights the importance of the level of irregularities.

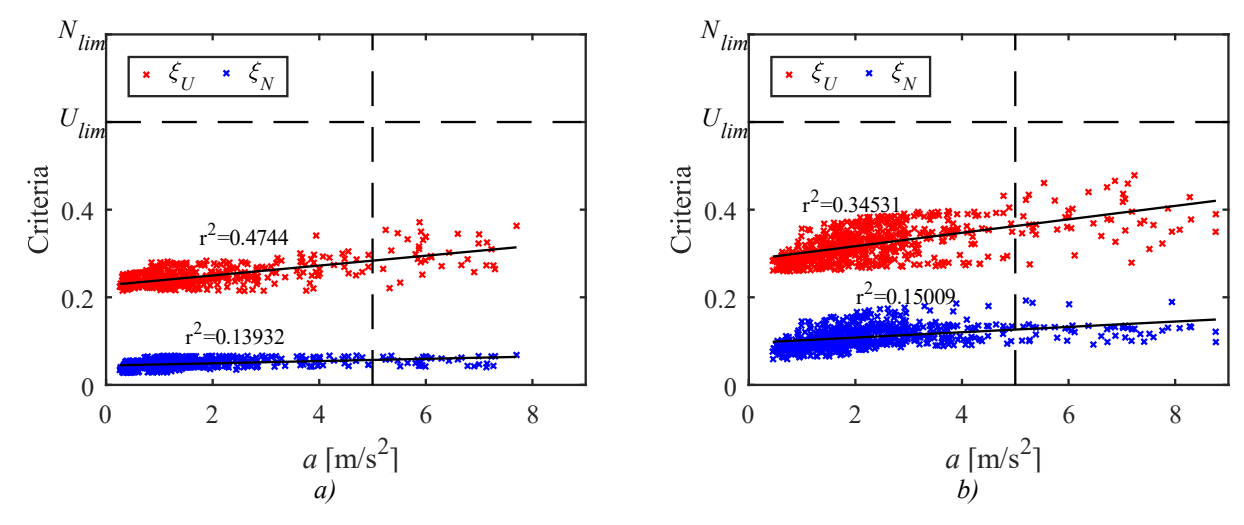


Figure 17: Relation between acceleration and derailment criteria (all bridges, every speed). a) every realization of a high-quality track; b) every realization of an Alert Limit track.



5.2 Additional analysis

5.2.1 Influence of increased irregularities

Results of the parametric analyses show that the derailment criteria are distant from their limits even at resonance. While deck acceleration is sensitive to both running speed and track condition, the Nadal and Unloading criteria are less influenced by the bridge's dynamic effects. An additional set of dynamic analyses is devised to sustain this observation further. These include generating new realizations of track irregularities, increasing both the vertical and alignment standard deviations in the 3 m to 25 m wavelength range, totalling 10 new profiles: 5 with a 50 % increase over the Alert limit's σ_{3-25} (named Alert×1.5) and 5 with 100 % increase (named Alert×2). This set of analyses was conducted on the 25 m bridge, with the HSLM-A3 model at 390 km/h, since this combination provided the most evident resonant situation.

Figure 18 presents the results from the increased irregularities simulations as boxplots superimposed on zoomed-in sections of Figure 14 d), Figure 15 d) and Figure 16 d). These figures allow for a comparison of 5 scenarios: smooth track, high-quality track, Alert Limit, 50 % increase of the Alert Limit and 100 % increase. It can be seen that there is a direct relation between a worse track and higher derailment criteria: maximum values registered include 0.704 for Unloading and 0.505 for Nadal. As for acceleration, a maximum value of 8.168 m/s² is measured.

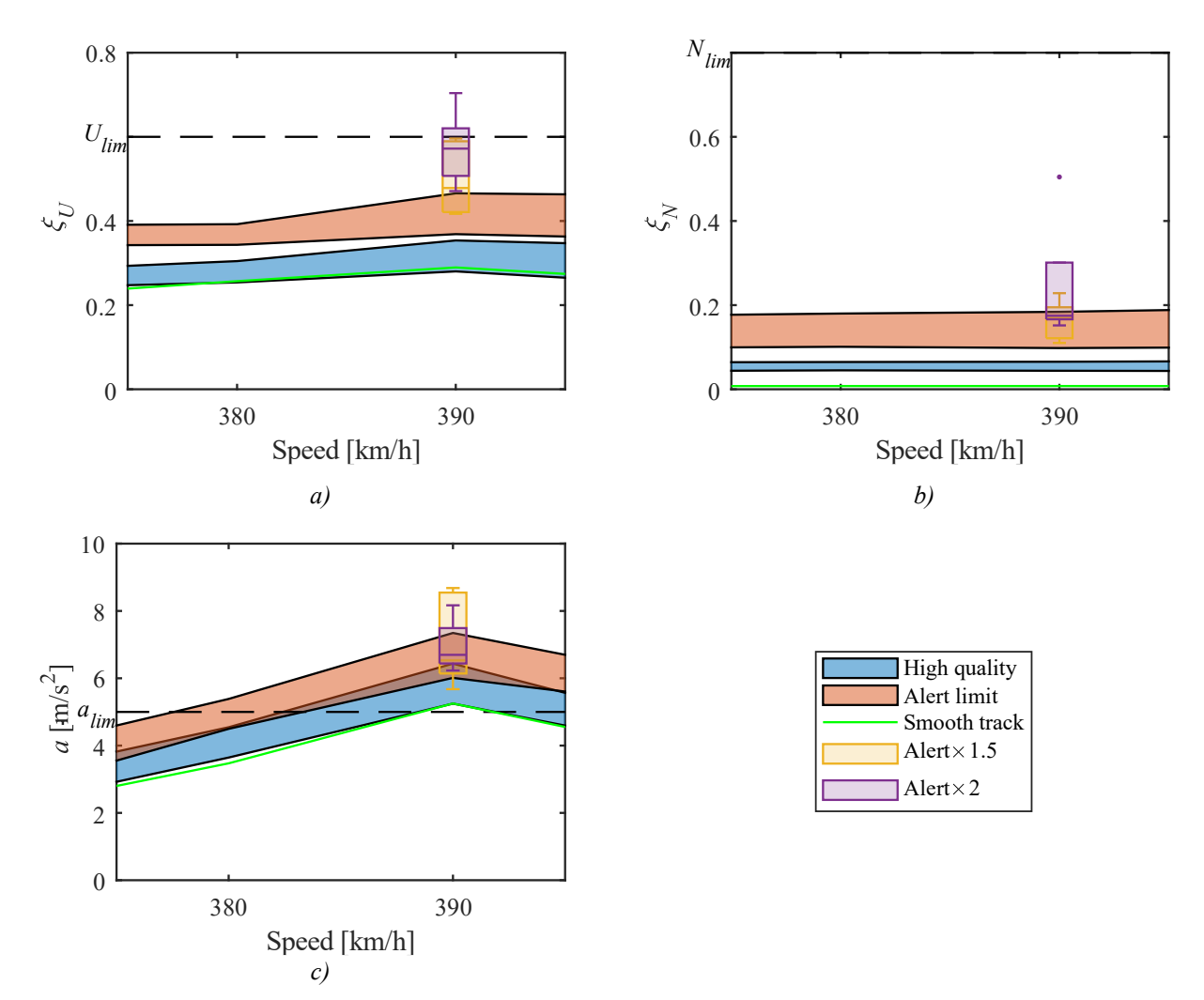


Figure 18: Criteria for increased irregularities on the 25 m bridge. a) Unloading; b) Nadal; c) Acceleration.

GA: 101121765 Work Package 5 Page | 26



The results presented strengthen the observation that derailment criteria, compared to deck accelerations, are more permeable to track conditions. It was necessary to increase Alert limit conditions up to double the standard deviation to register ξ_N values above 0.5 and ξ_U values greater than U_{lim} . On the other hand, acceleration was already greater than the normative 5 m/s² limit, even for a smooth track. Worsening the irregularity profiles increased the maximum acceleration. Still, it is worth noting that there is far more overlap between the different realizations' results on acceleration when compared to the derailment criteria, i.e., track condition plays a less relevant part in determining deck acceleration.

5.2.2 Influence of the bridge vibration

From either the parametric or the increased irregularities analyses, it can be inferred that track condition constitutes the predominant factor in assessing running safety. Even though the occurrence of resonance is relevant for deck acceleration, vibration from the bridge seems to have an imperceptible effect on the variation of wheel-rail contact forces and, therefore, on the derailment criteria. For this reason, the results of additional dynamic analyses of the same critical load model and speed as of the 25 m bridge, replacing it with a rigid bridge, are here presented. These simulations consider the 21 available profiles, i.e. the same employed for the increased irregularities analysis. Figure 19 depicts the distribution of results regarding the Unloading and Nadal criteria.

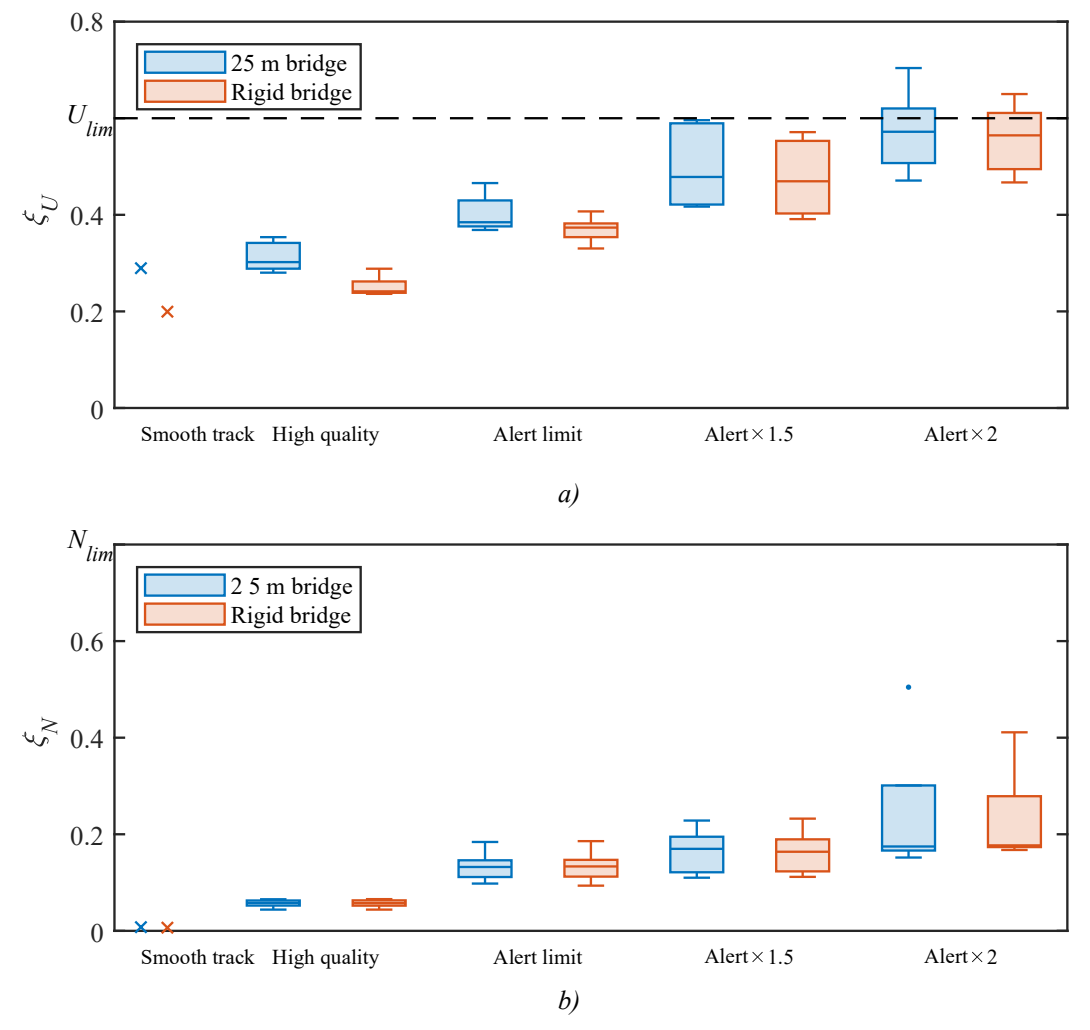


Figure 19: Influence of the bridge vibration. a) Unloading criterion; b) Nadal criterion.



The results indicate that regardless of considering the bridge's dynamic effects, the performance of derailment indicators is controlled by the track's condition. As quality decreases, so does the influence of the bridge vibration. To assess the fitness of using just the plain track model as a predictor (ξ_N^* and ξ_U^*) of the criteria, the sums of squared errors can be computed (using all available realizations) as:

$$\sum_{i=1}^{21} (\xi_U - \xi_U^*)^2 = 0.0419 \tag{9}$$

$$\sum_{i=1}^{21} (\xi_N - \xi_N^*)^2 = 0.0092 \tag{10}$$

Given that the scale of the criteria is between 0 and 1, the fact that the sums of squared errors are lower than 1 % makes them negligible. It can be concluded that regardless of the train model being subjected to bridge vibration, the relation between contact forces is already conditioned by the track quality.

5.2.3 Effect on riding comfort

The results of the analysis hitherto considered suggest that deck acceleration does not accurately relate to derailment criteria. Since running safety appears to be conditioned by track condition rather than the amount of bridge vibration, a revision of the Eurocode could result in removing the acceleration limit. However, even if the maximum deck acceleration does not portray running safety, its value should nevertheless be limited if it can be taken as an indicator for other measurements, such as riding comfort.

The present subsection measures passenger riding comfort by calculating the vertical acceleration at coach level b_v . Using the same case study bridges and track irregularity profiles, time histories are obtained for each carriage for the entire run (before, during, and after crossing the bridge), at every speed. These responses are band-pass filtered (0.4 Hz to 10 Hz, cut off at -3 dB), according to the "Ride characteristics" requirements in the EN 14363. The response section corresponding to the bridge crossing is isolated, and the maximum absolute value is stored. Figure 20 provides a visualization of these steps.

The envelopes containing the maximum coach acceleration are illustrated in Figure 21. The dataset comprises the results from each run's worst-performing coach. In the figures, the "Very good", "Good", and "Acceptable" thresholds correspond to the limits from the EN 1990. Similarly to the derailment criteria's analysis, it is observed that there is a clear separation concerning the track's quality, with the Alert limit tracks corresponding to the worst coach acceleration values. For high-quality tracks, the thinner envelopes indicate less dispersion in results, with their lower limits generally following the smooth tracks' results. In all five bridges, the Alert limit irregularities cause the riding comfort to cross the "Very good" line, with the 30 m bridge even demonstrating a crossing of the "Acceptable" line (albeit at very high speeds). A better-maintained high-quality track is not only less permeable to speed differences but also a guarantee of higher riding comfort.



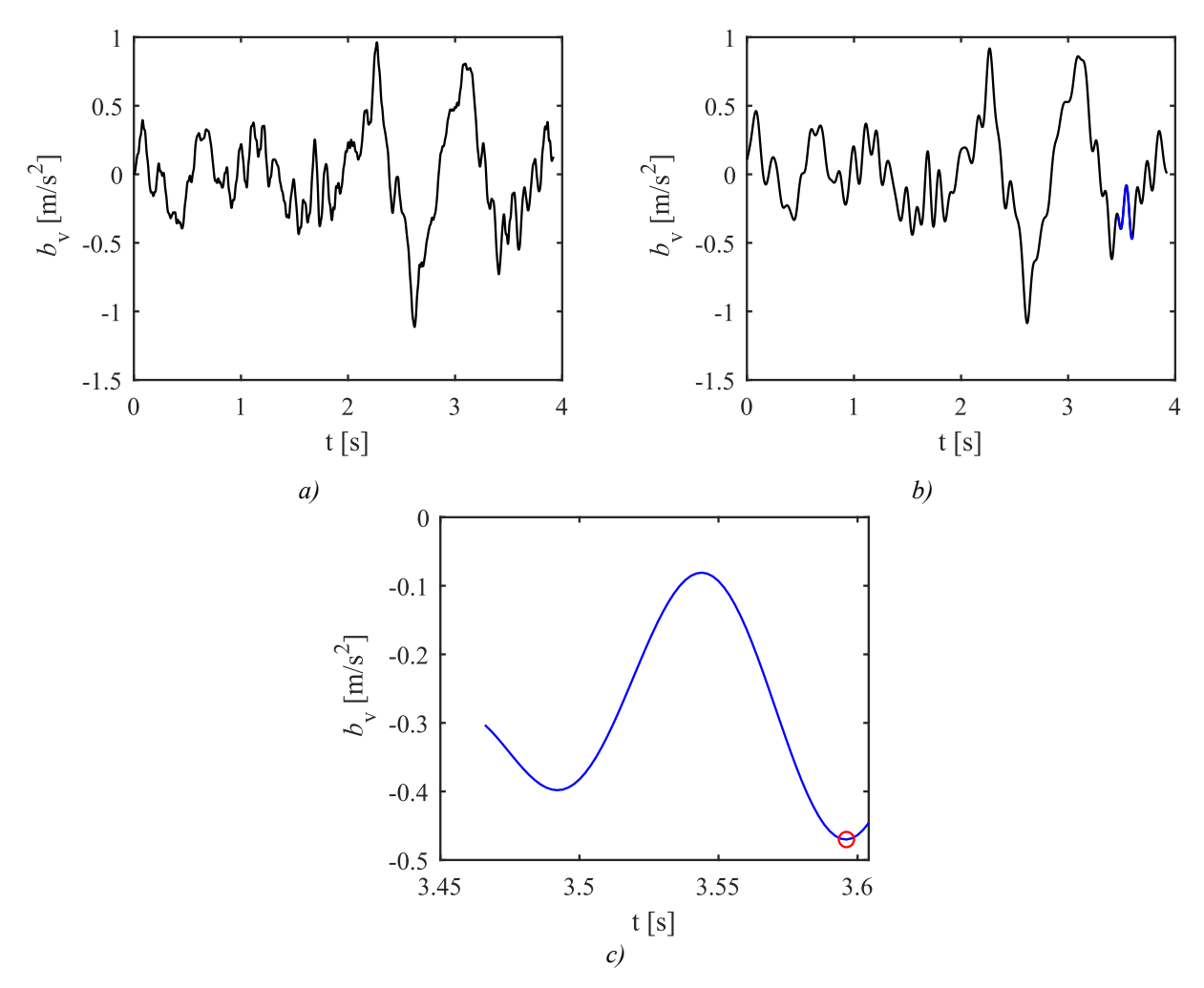


Figure 20: Visualization of the riding comfort assessment methodology. a) Entire time-history; b) Filtered response (bridge section in blue); c) Maximum absolute.

The possible correlation between deck and coach acceleration is further investigated by plotting the pairs of results (Figure 22) and calculating the coefficients of determination. There is less dispersion in the high-quality track results, which makes for a larger correlation than in the alert limit track results. Nonetheless, in high-quality tracks, deck accelerations around or above the normative limit of 5 m/s² do not increase coach acceleration. In fact, at 0.92 m/s², the maximum registered coach acceleration does not even cross the "Very good" 1 m/s² threshold. Conversely, in alert limit irregularity tracks, there are several instances where a deck acceleration of 6 m/s² can correspond either to a very low coach acceleration (0.47 m/s²) or up to values above (2.10 m/s²) the "Acceptable" threshold of 2 m/s². The correlation is insufficient to justify using deck acceleration as an indicator of passenger riding comfort.



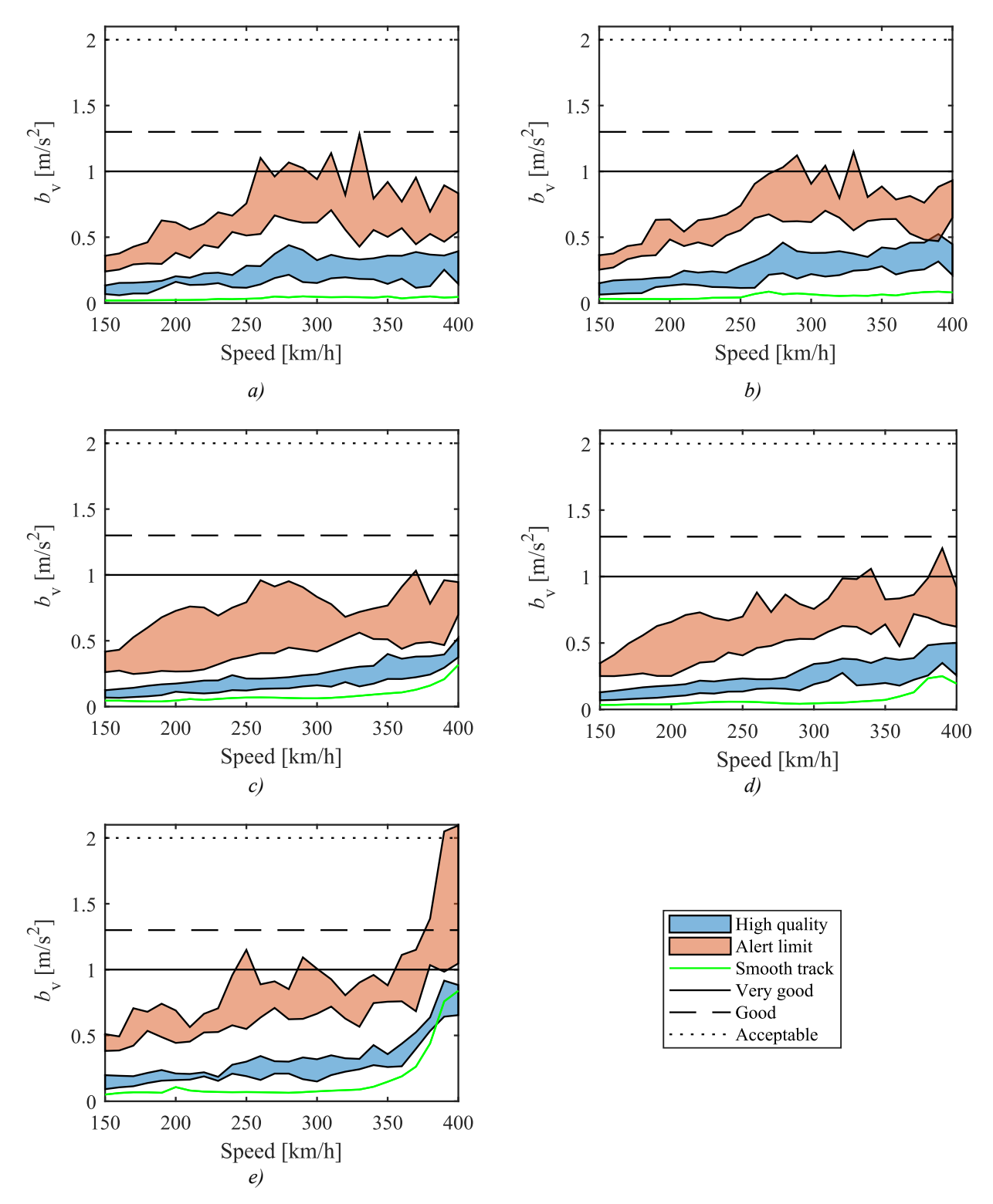


Figure 21: Coach acceleration envelopes. a) 10 m bridge; b) 15 m bridge; c) 20 m bridge; d) 25 m bridge; e) 30 m bridge.



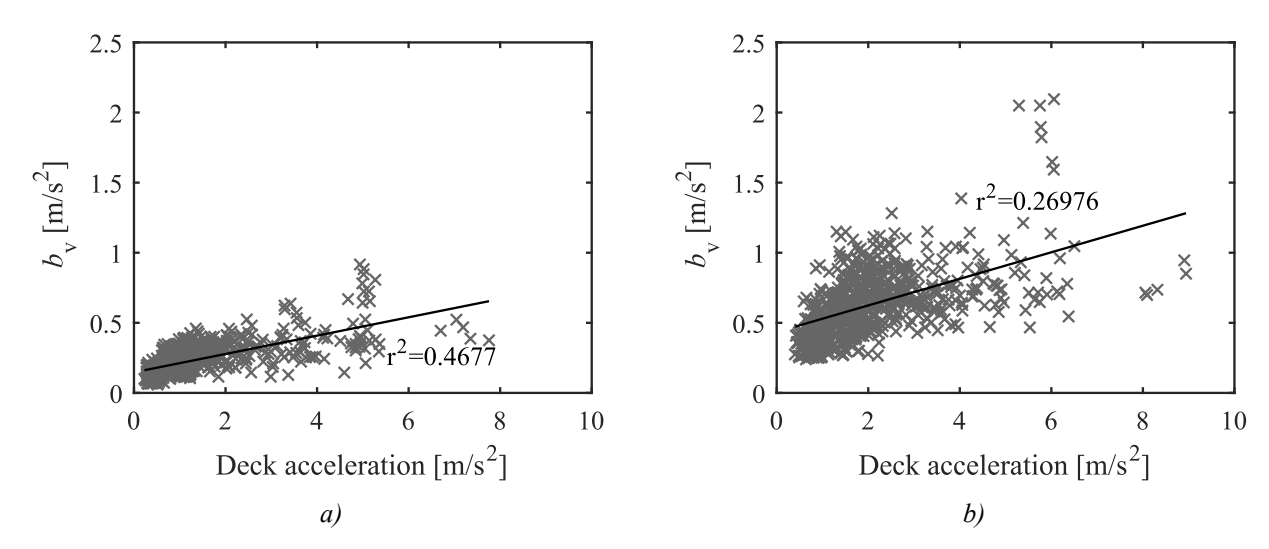


Figure 22: Relation between deck acceleration and coach acceleration (all bridges, every speed). a) every realization of a high-quality track; b) every realization of an Alert Limit track.

6 NORMATIVE RECOMMENDATION

6.1 Concluding remarks

This report addresses the pertinence of utilizing an acceleration limit as a conditioning factor for the dynamic design of railway bridges. Multiple realizations of two track quality levels were tested on a wide range of running speeds for five different bridges with train models representative of the HSLM-A. A comparative analysis of increased irregularities, as well as of the influence of the bridge vibration under resonance, was also presented to further sustain the observations. Acceleration at coach level was studied, evaluating its relation to deck acceleration.

It is found that ballastless railway bridges can experience acceleration values above the normative limit of 5 m/s² without it corresponding to a surpassing of derailment criteria, which does not support the thesis of using deck acceleration as a limiting factor for running safety. However, even though both the Unloading and the Nadal criteria present a low correlation with acceleration, the former does indicate a closer relation. Therefore, vertical dynamics are indispensable in assessing train running safety in scenarios when the Unloading criterion is conditioning. 3D analyses should be considered in scenarios where substantial lateral loads may contribute to the lateral instability of the train.

As for the importance of the track quality, across different running speeds, the Nadal criterion is shown to be close to constant, depending on the rail irregularities. The Unloading criterion is slightly more telling of the occurrence of resonance, while the acceleration values are greatly dependent on the train's speed. Results show that both derailment criteria are greatly influenced by the level of track quality, with bridge vibration being imperceptible for wheel-rail contact forces. For the study of derailment, track quality is far more relevant than the vibration experienced on the bridge. A similar observation is made regarding passenger comfort. The correlation between deck and coach acceleration across multiple bridges and running speeds is not strong enough to confidently infer the level of passenger riding comfort from the analysis of deck vertical acceleration.



6.2 Proposal for recommendation

The current Eurocode EN 1990 limits the maximum vertical deck acceleration to "prevent track instability, for traffic safety reasons". This relation is contested by the research presented in this report, which consistently suggests that vertical deck acceleration is unrelated to the assessment of running safety, concerning the occurrence of derailment. Not only is the current Eurocode limit of 5 m/s² not associated with any safety threshold, but deck acceleration itself, as an indicator, is insufficiently correlated to any variation in derailment criteria. Contrarily, track quality is a more relevant factor, demonstrating that the effect of rails' unevenness across hundreds of meters is far greater than the effect of the bridge's vibration. It could be argued, however, that deck acceleration should still have some limit value related to other non-safety-related phenomena. In this regard, this report presents an evaluation of whether riding comfort correlates with deck acceleration, yet the results do not point in that direction.

From the considerations presented, a lack of correlation between deck acceleration and derailment is noted, leading to the conclusion that the current normative limit might be over-conservative. Therefore, the normative recommendation for this matter is to remove the criterion presented in Section A.2.9.4.2.1 from the EN 1990 (CEN, 2023b), which limits the deck acceleration for ballastless track railway bridges to 5 m/s².

Nevertheless, dynamic assessment is still advisable since other limiting aspects may exist, such as support reaction and uplift, slab separation, deflection control, fatigue assessment, or relative rotation. Additionally, it should be noted that some acceleration limit could still exist due to the presence of loosely supported non-structural components or to prevent malfunctioning pantograph-catenary interaction (for instance, (Matsuoka et al., 2022) highlight the possible fatigue damage in overhead wires caused by excessive vibrations). However, such a limit should be clearly identified in the Eurocode as being due to the mentioned reasons (and to increase the serviceability of the bridge) and not because of traffic safety. In the case of future discussion and research work leading to the acceleration criterion being discarded, different limiting criteria should be tested and evaluated.

REFERENCES

- Allahvirdizadeh, R., Andersson, A., & Karoumi, R. (2022). Estimating running safety factor of ballastless railway bridges using tail modelling. *Acta Polytechnica CTU Proceedings*, *36*, 25–32. https://doi.org/10.14311/APP.2022.36.0025
- ANSYS®. (2018). Release 19.2. ANSYS Inc.
- Arvidsson, T., & Andersson, A. (2017). *Train-track-bridge interaction for non-ballasted railway bridges on high-speed lines* (No. TRITA-BKN Report 165). KTH Royal Institute of Technology. https://kth.diva-portal.org/smash/record.jsf?pid=diva2%3A1209473&dswid=-8418
- Arvidsson, T., Andersson, A., & Karoumi, R. (2018). Train running safety on non-ballasted bridges. *International Journal of Rail Transportation*, 7, 1–22.
- Cai, X., Guo, L., Hou, B., & Ren, C. (2016). Influence of ballastless track complex irregularities on high-speed train. *Beijing Jiaotong Daxue Xuebao/Journal of Beijing Jiaotong University*, 40(1), 12–19. https://doi.org/10.11860/j.issn.1673-0291.2016.01.002
- CEN. (2015). Railway applications—Track—Track geometry quality—Part 5: Geometric quality assessment. (No. EN 13848-5). Commité European de Normalisation (CEN):,.
- CEN. (2016). Railway applications—Testing and Simulation for the acceptance of running characteristics of railway vehicles—Running Behaviour and stationary tests (No. EN 14363). Commité European de Normalisation (CEN):,.



- CEN. (2023a). Eurocode 1—Actions on structures—Part 2: Traffic loads on bridges and other civil engineering works (No. EN 1991-2).
- CEN. (2023b). Eurocode—Basis of structural and geotechnical design (No. EN 1990). Commité European de Normalisation (CEN):,.
- Claus, H., & Schiehlen, W. (1998). Modeling and Simulation of Railway Bogie Structural Vibrations. *Vehicle System Dynamics*, 29(sup1), 538–552. https://doi.org/10.1080/00423119808969585
- ERRI D 202/RP 11. (1997). Parametric study and sensitivity analysis of CWERRI. European Rail Research Institute.
- ERRI D 214/RP 8. (1999). Rail bridges for speeds > 200 km/h: Confirmation of values against experimental data. European Rail Research Institute.
- European Commission. (2002, setembro). Consolidated text: Commission Decision of 30 May 2002 concerning the technical specification for interoperability relating to the infrastructure subsystem of the trans-European high-speed rail system referred to in Article 6(1) of Council Directive 96/48/EC (notified under document number C(2002) 1948) (Text with EEA relevance) (2002/732/EC) (p. 143). https://eur-lex.europa.eu/eli/dec/2002/732/2002-09-12
- European Union Agency for Railways. (2022). *ERA1193-TD-01-2022—ERA technical note on work needed* for closing TSI open points on bridge dynamics. https://rail-research.europa.eu:443/about-europes-rail/europes-rail-reference-documents/additional-technical-material/
- Ferreira, G., Montenegro, P., Andersson, A., Henriques, A. A., Karoumi, R., & Calçada, R. (2024). Critical analysis of the current Eurocode deck acceleration limit for evaluating running safety in ballastless railway bridges. *Engineering Structures*, 312, 118127. https://doi.org/10.1016/j.engstruct.2024.118127
- Goicolea, J. M. (2014). Simplified Mechanical Description of AVE S-103—ICE3 Velaro E High Speed Train. School of Civil Engineering, Technical University of Madrid–UPM. https://oa.upm.es/43946/
- Kalker, J. J. (1996). *Book of tables for the Hertzian creep-force law*. 2nd Mini Conference on Contact Mechanics and Wear of Wheel/Rail Systems, Budapest, Hungary.
- Lee, Y.-S., & Kim, S.-H. (2010). Structural analysis of 3D high-speed train—bridge interactions for simple train load models. *Vehicle System Dynamics*, 48(2), 263–281. https://doi.org/10.1080/00423110902751912
- Ling, L., Dhanasekar, M., Wang, K., Zhai, W., & Weston, B. (2019). Collision derailments on bridges containing ballastless slab tracks. *Engineering Failure Analysis*, 105, 869–882. https://doi.org/10.1016/j.engfailanal.2019.07.042
- MATLAB®. (2018). R2018a. The Mathworks, Inc.
- Matsuoka, K., Tsunemoto, M., & Tokunaga, M. (2022). Dynamic behaviour of railway poles built on bridges under train passage in high-speed railways and a simple evaluation method. *Engineering Structures*, 257, 114099. https://doi.org/10.1016/j.engstruct.2022.114099
- Moliner, E., Martínez-Rodrigo, M. D., & Museros, P. (2017). Dynamic performance of existing double track railway bridges at resonance with the increase of the operational line speed. *Engineering Structures*, 132, 98–109. https://doi.org/10.1016/j.engstruct.2016.11.031
- Montenegro, P., Barbosa, D., Carvalho, H., & Calçada, R. (2020). Dynamic effects on a train-bridge system caused by stochastically generated turbulent wind fields. *Engineering Structures*, *211*, 110430. https://doi.org/10.1016/j.engstruct.2020.110430
- Montenegro, P., Carvalho, H., Ortega, M., Millanes, F., Goicolea, J. M., Zhai, W., & Calçada, R. (2022). Impact of the train-track-bridge system characteristics in the runnability of high-speed trains against crosswinds—Part I: Running safety. *Journal of Wind Engineering and Industrial Aerodynamics*, 224, 104974. https://doi.org/10.1016/j.jweia.2022.104974



- Montenegro, P., Carvalho, H., Ribeiro, D., Calçada, R., Tokunaga, M., Tanabe, M., & Zhai, W. (2021). Assessment of train running safety on bridges: A literature review. *Engineering Structures*, 241, 112425. https://doi.org/10.1016/j.engstruct.2021.112425
- Montenegro, P., Neves, S., Calçada, R., Tanabe, M., & Sogabe, M. (2015). Wheel-rail contact formulation for analyzing the lateral train-structure dynamic interaction. *Computers & Structures*, 152, 200–214.
- National Railway Administration of the People's Republic of China. (2017). *Code for Design on Railway Bridge and Culvert, TB 10002-2017*. National Railway Administration of the People's Republic of China
- Neto, J., Montenegro, P., Vale, C., & Calçada, R. (2021). Evaluation of the train running safety under crosswinds—A numerical study on the influence of the wind speed and orientation considering the normative Chinese Hat Model. *International Journal of Rail Transportation*, *9*(3), 204–231. https://doi.org/10.1080/23248378.2020.1780965
- Neves, S. G. M., Montenegro, P., Azevedo, A. F. M., & Calçada, R. (2014). A direct method for analyzing the nonlinear vehicle–structure interaction. *Engineering Structures*, 69, 83–89. https://doi.org/10.1016/j.engstruct.2014.02.027
- Railway Technical Research Institute. (2006). Outline of design standards for railway structures and commentary (displacement limits). Maruzen Co., Ltd.
- Shi, H., Yu, Z., & Shi, H. (2016). *An improved method for dynamic modelling of a slab track on a high-speed railway*. 225–237. https://doi.org/10.2495/CR160211
- Yang, Y. B., & Yau, J. D. (2017). Resonance of high-speed trains moving over a series of simple or continuous beams with non-ballasted tracks. *Engineering Structures*, 143, 295–305. https://doi.org/10.1016/j.engstruct.2017.04.022
- Zacher, M., & Baeßler, M. (2008). Dynamic behaviour of ballast on railway bridges. Em *Dynamics of High–Speed Railway Bridges. Selected and Revised Papers from the Advanced Course on 'Dynamics of High–Speed Railway Bridges', Porto, Portugal, 20–23 September 2005* (pp. 125–142). CRC Press. https://www.taylorfrancis.com/chapters/edit/10.1201/9780203895405-11/dynamic-behaviour-ballast-railway-bridges-zacher-bae%C3%9Fler
- Zhai, W., Liu, P., Lin, J., & Wang, K. (2015). Experimental investigation on vibration behaviour of a CRH train at speed of 350 km/h. *International Journal of Rail Transportation*, 3(1), 1–16. https://doi.org/10.1080/23248378.2014.992819